by glucose loading (Fig. 1*G*). While the intraperitoneal administration of histidine alone did not significantly change blood glucose levels, it significantly downregulated the expression of the *G6pc* gene, which encodes G6Pase, with and without glucose loading (Fig. 1*H*). However, the expression of the *Pck1* gene, which encodes PEPCK, did not change significantly after the intraperitoneal administration of histidine alone or with glucose. The administration of fructose and pyruvate is known to increase blood glucose levels mildly through gluconeogenesis (20,21); however, histidine

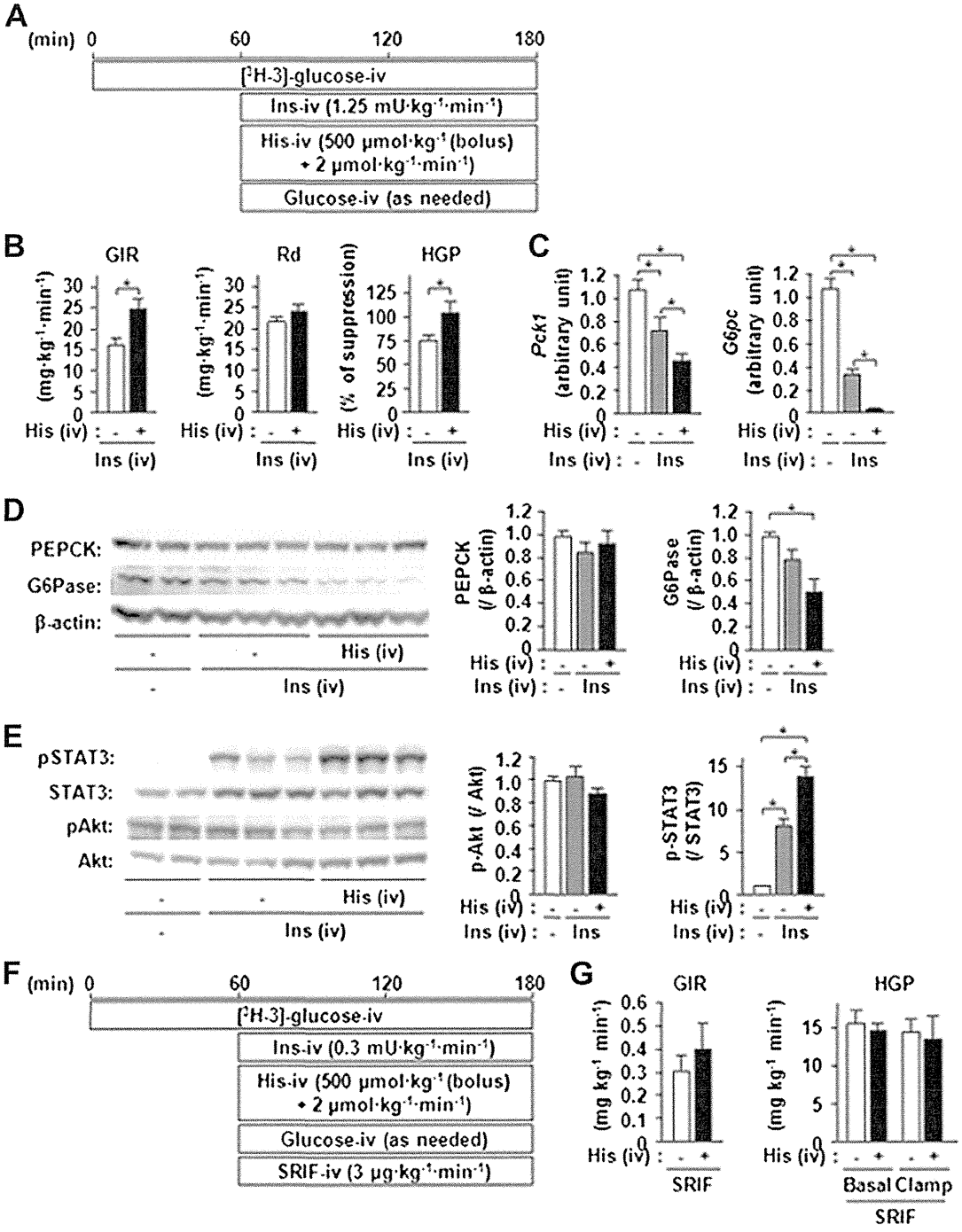

FIG. 2. Augmentation of the insulin-dependent suppression of HGP by histidine. *A*: Schematic of hyperinsulinemic-euglycemic clamping with continuous intravenous administration of histidine (His) or saline (-). *B* and *C*: GIR (*B*, *left panel*), R_d (*B*, *center panel*), and the suppression (%) of HGP (*B*, *right panel*) in the study described in *A*. Quantitative PCR analysis of *Pck1* and *G6pc* gene expression levels in the liver is shown in *C*. $^*P < 0.05$ (n = 7–9). *D* and *E*: Western blotting was performed to analyze the levels of hepatic PEPCK, G6Pase, and β-actin (*D*) and phosphorylation of STAT3 and Akt (*E*) at 120 min after insulin (Ins) administration in the hyperinsulinemic-euglycemic clamp study (*A*). Quantitation of PEPCK and G6Pase levels is normalized to β-actin (*D*). Quantitation of phospho-Akt and phospho-STAT3 is normalized to Akt and STAT3, respectively (*E*). Data are represented as means ± SE (n = 7–9) values. *F*: Schematic of euglycemic-pancreatic clamp tests with continuous intravenous administration of histidine or saline in addition to somatostatin injection. *G*: The GIR (*left panel*) and the suppression (%) of HGP (*right panel*) in the study described in *F* (n = 5).

injection attenuated the increase in blood glucose levels after the administration of fructose (Fig. 1*I*) and pyruvate (Fig. 1*J*).

Histidine administration augments the insulin-induced suppression of HGP. We used a hyperinsulinemic-euglycemic clamp technique to investigate the effect of histidine on HGP (Fig. 2*A*). The GIR and the suppression rate of HGP obtained after insulin administration were increased by histidine administration (Fig. 2*B*). The suppression of hepatic gene expression of *Pck1* and *G6pc* by insulin was augmented by histidine (Fig. 2*C*), even though histidine did not affect plasma insulin levels in the clamp tests (Supplementary Fig. 1). While PEPCK protein expression did not change significantly during the 120-min hyperinsulinemic-euglycemic clamping period, insulin administration reduced the levels of G6Pase protein, and this reduction was

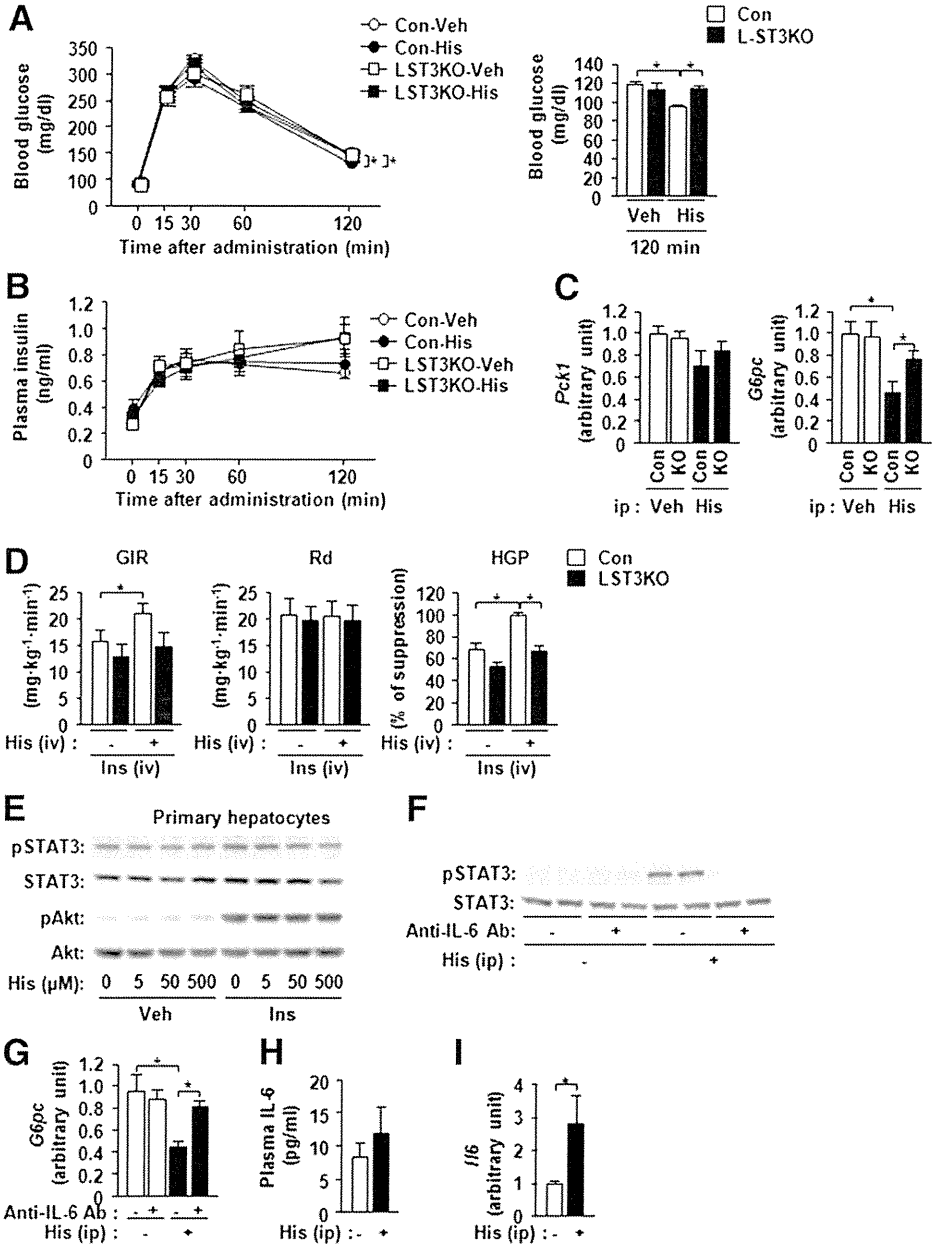

FIG. 3. Activation of hepatic IL-6/STAT3 signaling pathways is required for the histidine-mediated regulation of HGP. *A* and *B*: A glucose tolerance test was conducted after the intraperitoneal injection of histidine (His) in liver-specific STAT3-deficient (LST3KO) mice and controls (Con). Changes in blood glucose levels (*A*, *left panel*), blood glucose levels at 120 min after glucose loading (*A*, *right panel*), and changes in plasma insulin levels (*B*) are shown. $^*P < 0.05$ ($n = 10$). *C*: Expression of hepatic *Pck1* and *G6pc* genes was analyzed by quantitative PCR at 120 min after the intraperitoneal injection of His into LST3KO and control (Con) mice. $^*P < 0.05$ ($n = 6$–8). *D*: Hyperinsulinemic-euglycemic clamping was conducted as described in Fig. 2*A*. The GIR (*left panel*), R_d (*center panel*), and suppression (%) of HGP (*right panel*) were measured. $^*P < 0.05$ ($n = 6$). *E*: Primary hepatocytes were treated with the different concentrations of histidine and insulin (Ins) shown in the figure, and the phosphorylation of STAT3, Akt, p70 S6 kinase, and S6 ribosomal protein was analyzed. *F*–*I*: The effect of intraperitoneal histidine injection on liver function was investigated using an IL-6 neutralizing antibody. *F*: Phosphorylation of hepatic STAT3 was analyzed by Western blotting at 120 min after histidine administration. *G*–*I*: Hepatic *G6pc* gene expression (*G*), blood IL-6 levels (*H*), and hepatic *Il6* gene expression (*I*) at 120 min after histidine administration are shown. $^*P < 0.05$ ($n = 7$–9).

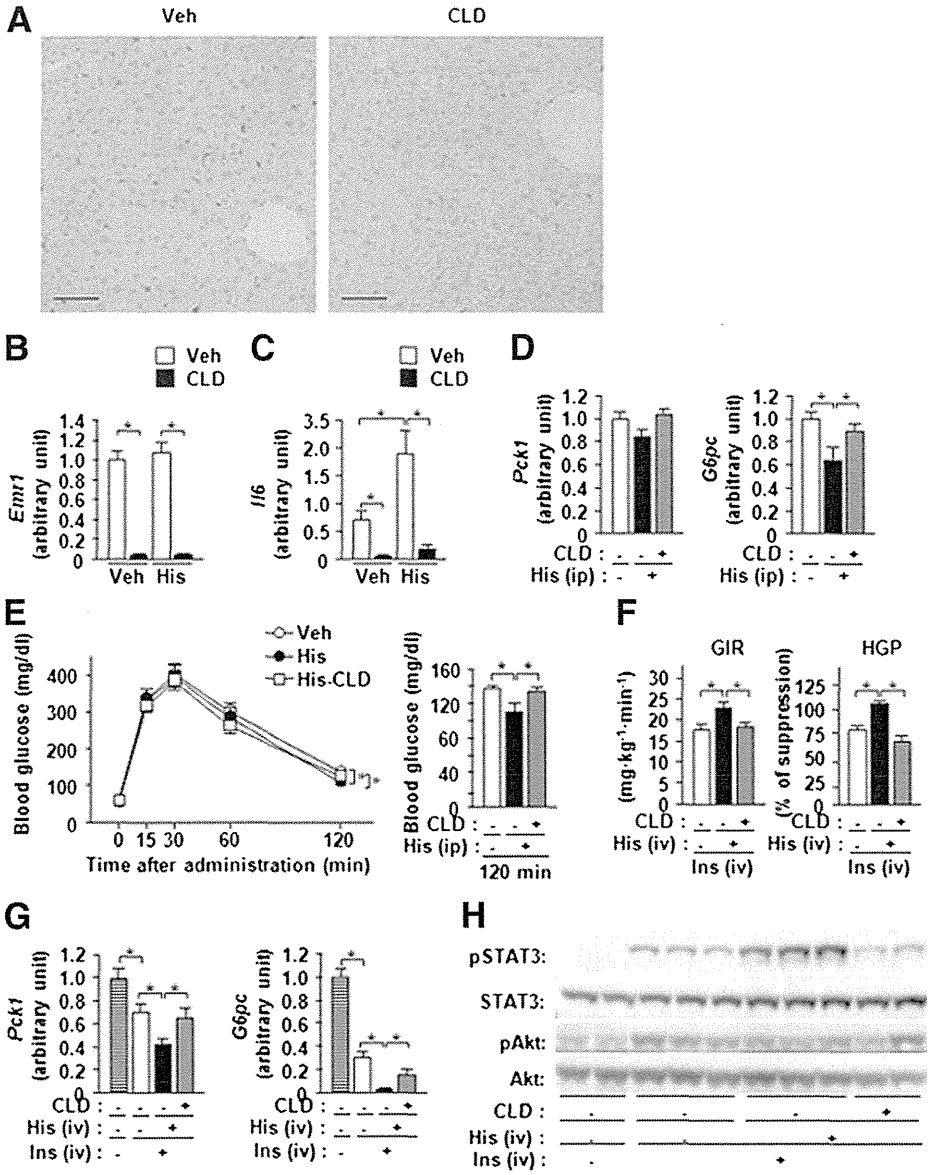

FIG. 4. Liver Kupffer cells are essential for the regulation of HGP by histidine (His). *A*: Immunostaining with an anti-Mac-2 antibody was performed in Kupffer cells after the administration of CLD. Scale bars, 50 nm. *B–D*: Histidine was injected intraperitoneally into mice pretreated with CLD, and *Emr1* (*B*), *Il6* (*C*), and *Pck1* and *G6pc* (*D*) gene expression in the liver was quantitated using PCR at 120 min after histidine administration. **P* < 0.05 (*n* = 5–7). *E*: The intraperitoneal injection of histidine and a glucose tolerance test were conducted in mice pretreated with CLD. Changes in blood glucose levels (*E*, *left panel*) and blood glucose levels at 120 min after glucose loading (*E*, *right panel*) are shown. **P* < 0.05 (*n* = 9). *F–H*: With the continuous administration of histidine, hyperinsulinemic-euglycemic clamping (Fig. 2*A*) was performed in mice pretreated with CLD, and the GIR (*left panel*) and suppression (%) of HGP (*right panel*) were measured. In addition, the expression of hepatic *Pck1* and *G6pc* genes (*G*) and the phosphorylation of hepatic STAT3 and Akt (*H*) at 120 min after insulin (Ins) administration were examined. **P* < 0.05 (*n* = 6).

augmented by histidine administration (Fig. 2*D*). Phosphorylation of STAT3, but not Akt, was observed at 120 min after insulin administration (Fig. 2*E*), and histidine enhanced the phosphorylation of STAT3 caused by hyperinsulinemia (Fig. 2*E*). To evaluate the histidine effect of HGP with fasting levels of insulin, we performed euglycemic-pancreatic clamp tests (Fig. 2*F*). No significant changes in GIR or HGP resulted from the presence or absence of histidine injection (Fig. 2*G*).

Activation of hepatic IL-6/ STAT3 signaling pathways essential for the histidine-mediated regulation of hepatic glucose metabolism. We investigated the significance of hepatic STAT3 in the suppression of HGP after histidine administration using 8- to 10-week-old LST3KO mice, which had not yet developed insulin resistance (5). In a glucose tolerance test with histidine administration, blood glucose levels were significantly decreased in the control, but not LST3KO, mice at 120 min after glucose loading (Fig. 3*A*), even though no significant difference in plasma insulin levels was observed between the groups (Fig. 3*B*). While *G6pc* gene expression was downregulated at 120 min after the intraperitoneal administration of histidine in the control mice, no such downregulation was observed in the LST3KO mice (Fig. 3*C*). In the hyperinsulinemic-euglycemic clamp tests, histidine increased the GIR and the suppression of HGP caused by insulin administration

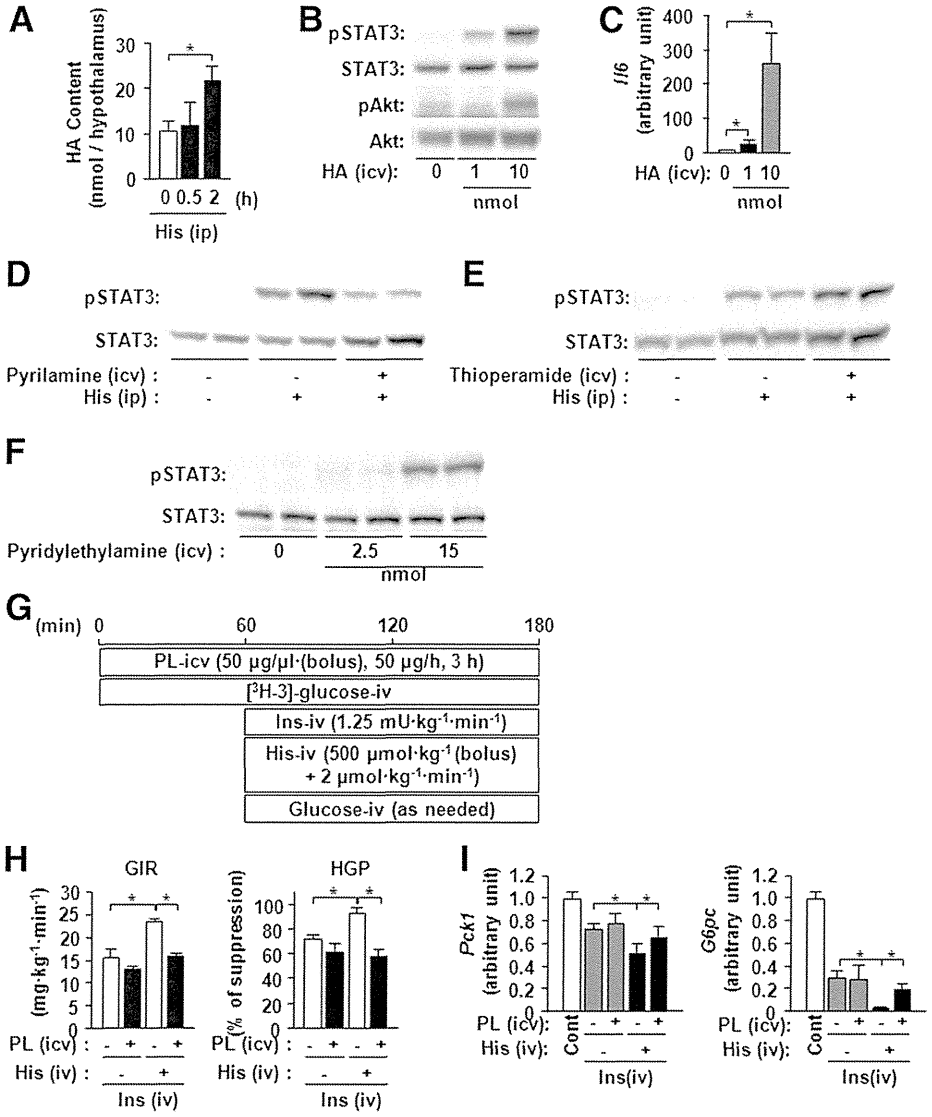

FIG. 5. Central histamine action is required for the regulation of HGP by histidine. *A*: Hypothalamic histamine (HA) content was measured at 30 and 120 min after the intraperitoneal administration of histidine (His). **P* < 0.05 (*n* = 5). *B* and *C*: HA was injected into the ventricle at the concentrations shown in the figure, and the phosphorylation of hepatic STAT3 and Akt (*B*) and expression of hepatic *Il6* gene (*C*) were analyzed at 180 min postadministration. **P* < 0.05 (*n* = 5). *D*: Histidine was injected intraperitoneally at 15 min after the lateral ventricular administration of the histamine H_1 receptor antagonist pyrilamine (50 µg/mouse), and phosphorylation of hepatic STAT3 was analyzed at 120 min after histidine administration. *E*: The intraperitoneal administration of histidine was performed at 30 min after the lateral ventricular administration of the histamine H_3 receptor antagonist thioperamide (50 nmol/mouse), and phosphorylation of hepatic STAT3 was analyzed at 120 min after histidine administration. *F*: Phosphorylation of hepatic STAT3 was analyzed (*n* = 4) at 180 min after the lateral ventricular administration of the histamine H_1 receptor agonist pyridylethylamine at the concentrations indicated in the figure. *G–I*: A hyperinsulinemic-euglycemic clamp (Ins injection) was performed with the continuous administration of histidine (His) or saline (-) in the jugular vein and pyrilamine (PL) or artificial cerebrospinal fluid (-) in the lateral ventricle, as shown in the schematic (*G*). The GIR (*H, left panel*) and the suppression (%) of HGP (*H, right panel*) are shown. ANOVA for GIR (*H, left panel*) revealed a significant effect of pyrilamine and histidine, as well as an interaction between pyrilamine and histidine (*P* < 0.05, *n* = 6). ANOVA for HGP (*H, right panel*) revealed a significant main effect of pyrilamine (*P* < 0.05) and an interaction between pyrilamine and histidine (*P* < 0.01, *n* = 6). In addition, the expression of hepatic *Pck1* and *G6pc* genes was analyzed at 120 min after insulin administration (*I*). **P* < 0.05 (*n* = 6). Cont, control.

in the control animals but not in the LST3KO mice (Fig. 3*D*). Insulin activates hepatic STAT3 via the central nervous system and the subsequent upregulation of *Il6* gene expression in the liver (9). Indeed, not only insulin but also histidine failed to activate STAT3 in primary hepatocytes (Fig. 3*E*). Histidine also had no effect on the Akt and S6 kinase pathway (Fig. 3*E*). Therefore, we used an IL-6 neutralizing antibody to investigate the role of IL-6 in the histidine-mediated activation of hepatic STAT3. The administration of the anti–IL-6 antibody prior to histidine administration attenuated the histidine-induced phosphorylation of STAT3 (Fig. 3*F*) as well as the suppression of *G6pc* gene expression (Fig. 3*G*). Histidine administration did not significantly change the plasma levels of IL-6 (Fig. 3*H*) but significantly upregulated *Il6* gene expression in the liver (Fig. 3*I*). These results suggest that, similar to insulin, histidine activates hepatic STAT3 through the upregulation of hepatic IL-6.

Kupffer cells are essential for the histidine-mediated regulation of hepatic glucose metabolism. In the liver, Kupffer cells play an important role in the production of

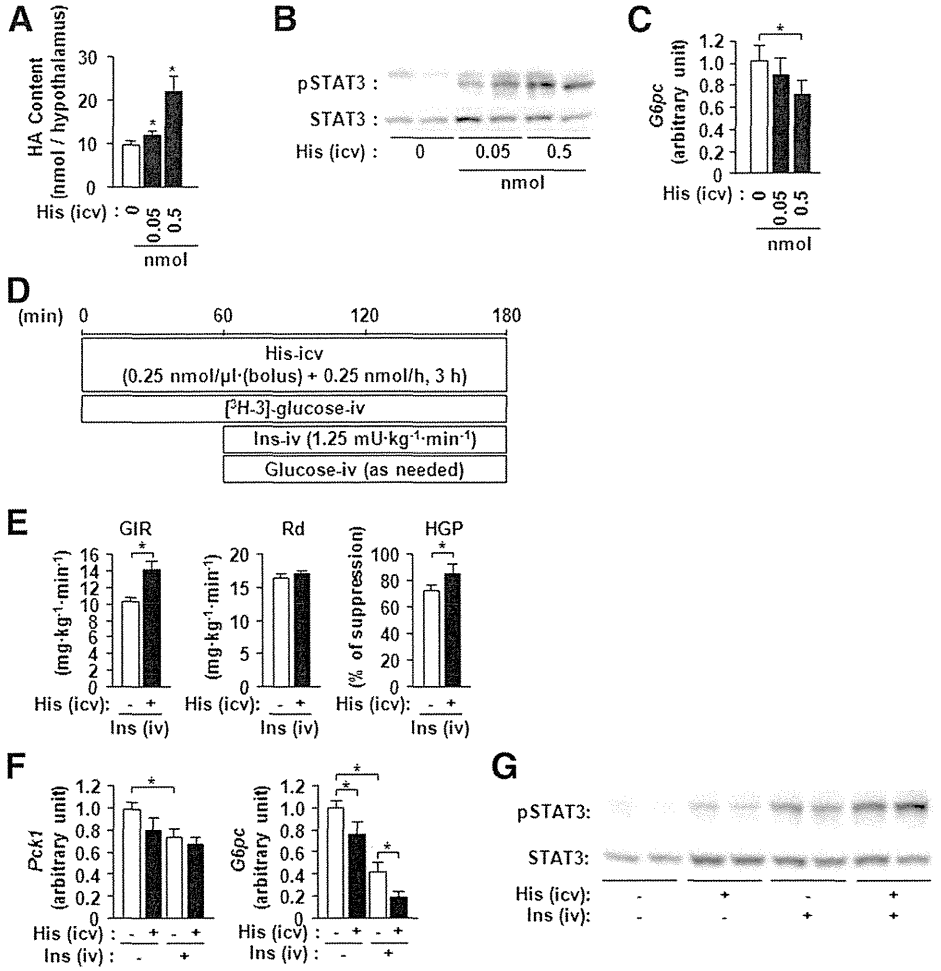

FIG. 6. ICV administration of histidine (His) augments the insulin-dependent suppression of HGP. *A–C*: With use of the doses indicated in the figure, histidine was injected rapidly into the lateral ventricle, and hypothalamic histamine (HA) content (*A*), phosphorylation of hepatic STAT3 (*B*), and expression of the hepatic *G6pc* gene (*C*) were analyzed at 180 min postadministration. *$P < 0.05$ ($n = 5$–8). *D–G*: As shown in the schematic (*D*), hyperinsulinemic-euglycemic clamping was performed concurrently with the continuous administration of histidine or artificial cerebrospinal fluid (-) into the lateral ventricle. The GIR (*E, left panel*), R_d (*E, center panel*), and suppression (%) of HGP (*E, right panel*) were measured. *$P < 0.05$ ($n = 6$). In addition, the expression of hepatic *Pck1* and *G6pc* genes (*F*) and phosphorylation of hepatic STAT3 (*G*) were analyzed at 120 min after insulin administration. ANOVA for *Pck1* (*F, left panel*) revealed a significant main effect of Ins ($P < 0.05$) but no significant interaction between Ins and His ($P = 0.060$, $n = 6$). ANOVA for *G6pc* (*F, right panel*) revealed a significant main effect of Ins and histidine ($P < 0.05$), but no significant interaction between insulin and histidine treatments ($P = 0.120$, $n = 6$).

IL-6 (22,23); therefore, we depleted Kupffer cells by the intravenous injection of CLD and investigated the function of histidine (22). CLD administration resulted in the disappearance of Mac-2–positive cells (Fig. 4*A*) and significantly downregulated the expression of the *Emr1* gene (Fig. 4*B*), which is specific to Kupffer cells in the liver. In addition, the depletion of Kupffer cells diminished the expression of hepatic *Il6* (Fig. 4*C*). Histidine administration, which significantly downregulates the expression of the hepatic *G6pc* gene, did not change its expression after CLD administration (Fig. 4*D*). In the glucose tolerance test, histidine administration significantly reduced blood glucose levels at 120 min after glucose loading; however, this reduction was diminished after CLD administration (Fig. 4*E*). In a hyperinsulinemic-euglycemic clamp experiment, histidine augmented the effects of insulin on *Pck1* and *G6pc* gene expression, HGP, and the GIR, but the augmentation of insulin action by histidine was diminished by CLD administration (Fig. 4*F* and *G*). Although histidine augmented the STAT3 phosphorylation caused by hyperinsulinemia, this augmentation was attenuated by CLD administration (Fig. 4*H*). These results indicate that hepatic IL-6 expression in Kupffer cells is essential for the histidine-mediated regulation of hepatic glucose metabolism.

Central histamine mediates the regulation of hepatic glucose metabolism by histidine. Histidine is a precursor of histamine; therefore, the levels of histamine in the hypothalamus are reportedly increased after the systemic administration of histidine (24,25). Thus, we investigated the involvement of central histamine in the histidine-mediated activation of hepatic STAT3 and regulation of HGP. As reported previously, histidine administration increased the levels of histamine in the hypothalamus (Fig. 5*A*). In addition, the ICV administration of histamine induced the phosphorylation of hepatic STAT3 (Fig. 5*B*) and upregulated the expression of *Il6* in the liver (Fig. 5*C*). The lateral ventricular administration of the histamine H_1 receptor antagonist pyrilamine prior to systemic histidine administration attenuated the phosphorylation of hepatic STAT3 (Fig. 5*D*), whereas the ICV administration of the histamine

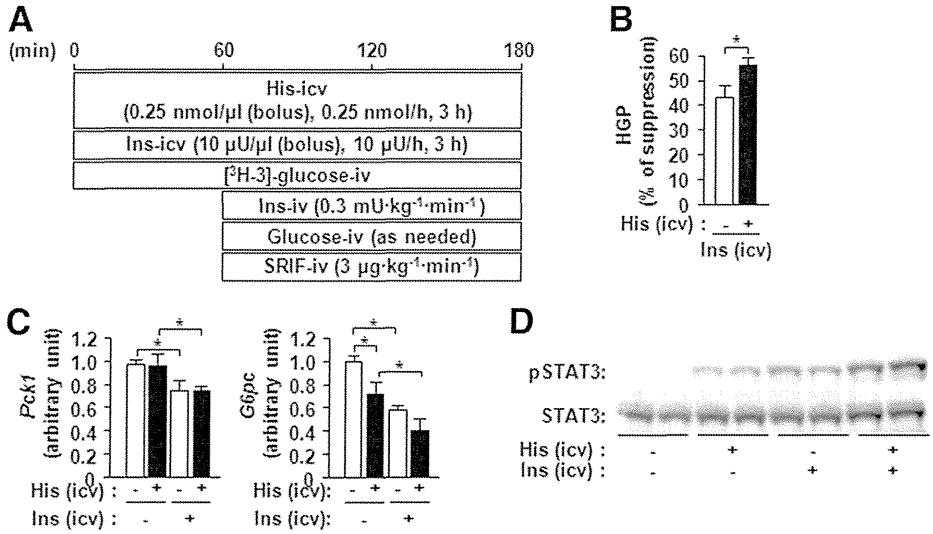

FIG. 7. Central histidine (His) action augments the suppression of HGP by insulin ICV administration. ***A–D*****: As shown in the schematic (*A*), continuous lateral ventricular injection of histidine, artificial cerebrospinal fluid (aCSF) (-), and insulin (Ins) in pancreatic clamping was performed. The suppression (%) of HGP, *$P < 0.05$ ($n = 6$) (*B*), expression of hepatic *Pck1* and *G6pc* genes at 180 min after the start of lateral ventricular administration (*C*), and phosphorylation of hepatic STAT3 (*D*) were analyzed. ANOVA for *Pck1* expression (*C*, *left panel*) revealed a significant main effect of Ins ($P < 0.05$) but no significant interaction between insulin and histidine ($P = 0.964$, $n = 6$). ANOVA for *G6pc* expression (*C*, *right panel*) revealed a significant main effect of insulin and histidine ($P < 0.05$) but no significant interaction between insulin and histidine treatments ($P = 0.116$, $n = 6$).**

H3 receptor antagonist thioperamide increased STAT3 phosphorylation (Fig. 5*E*). Conversely, the ICV administration of the histamine H_1 receptor agonist pyridylethylamine activated hepatic STAT3 (Fig. 5*F*). To elucidate the role of central histamine/histamine H_1 receptor in the histidine-mediated regulation of HGP, we performed a hyperinsulinemic-euglycemic clamp study with the concurrent ICV administration of pyrilamine and intravenous administration of histidine (Fig. 5*G*). Although histidine administration augmented the action of insulin on *Pck1* and *G6pc* gene expression, HGP, and the GIR, the ICV administration of pyrilamine blocked this augmentation (Fig. 5*H* and *I*).

ICV administration of histidine augments the insulin-dependent suppression of HGP. We administered histidine into the ventricle to investigate the involvement of the central-mediated regulation of HGP by histidine. As with intraperitoneal injection, the ICV administration of histidine increased the hypothalamic histamine content (Fig. 6*A*). In addition, histidine ICV administration upregulated the phosphorylation of hepatic STAT3 (Fig. 6*B*) and suppressed *G6pc* gene expression in the liver (Fig. 6*C*). We then investigated the effect of histidine ICV administration on the insulin-dependent suppression of HGP (Fig. 6*D*). In hyperinsulinemic-euglycemic clamping, the ICV administration of histidine increased the GIR and augmented the suppression of HGP (Fig. 6*E*). The ICV administration of histidine suppressed the expression of the *G6pc* gene and augmented the suppression of gene expression by the systemic administration of insulin (Fig. 6*F*), whereas *Pck1* gene expression tended to decrease, albeit insignificantly, after histidine administration (Fig. 6*F*). Furthermore, histidine ICV administration increased the phosphorylation of hepatic STAT3 and additively enhanced the hepatic phosphorylation of STAT3 associated with hyperinsulinemia (Fig. 6*G*). These results indicate that the suppression of HGP by the systemic administration of insulin is augmented by the central administration of histidine.

We then injected insulin and histidine into the ventricle to investigate the effect of central histidine on the regulation of HGP by central insulin action (Fig. 7*A*). The ICV administration of insulin was performed with the concurrent administration of somatostatin to block the secretion of endogenous insulin caused by insulin ICV administration (Fig. 7*A*). As reported previously, the ICV administration of insulin suppressed HGP, while the ICV administration of histidine augmented this suppression (Fig. 7*B*). In addition, with the ICV administration of insulin the expression of the *Pck1* gene decreased, albeit insignificantly, whereas the expression of the *G6pc* gene was significantly downregulated (Fig. 7*C*). Histidine administration augmented the suppression of *G6pc* gene expression (Fig. 7*C*). Hepatic STAT3 was phosphorylated after the ICV administration of insulin or histidine, and their coadministration enhanced its phosphorylation (Fig. 7*D*). These results indicate that the central administration of histidine augments the suppression of HGP by central insulin action.

Central histidine action is independent of central insulin action. Next, we investigated the cross-talk between central histidine and central insulin action, both of which activate hepatic STAT3. As pyrilamine administration inhibited hepatic STAT3 phosphorylation mediated by the systemic administration of histidine (Fig. 5*D*), the phosphorylation of hepatic STAT3 was attenuated by the administration of pyrilamine prior to the ICV administration of histidine (Fig. 8*A*). Conversely, the phosphorylation of hepatic STAT3 induced by the ICV administration of insulin was not altered by the preadministration of pyrilamine (Fig. 8*B*). Furthermore, in a study using Hrh1KO mice (16) the phosphorylation of hepatic STAT3 was significantly attenuated after the ICV administration of histidine (Fig. 8*C*) in the same manner as that after pyrilamine administration. However, no significant change in hepatic STAT3 phosphorylation was induced by the ICV administration of insulin to the Hrh1KO mice (Fig. 8*D*).

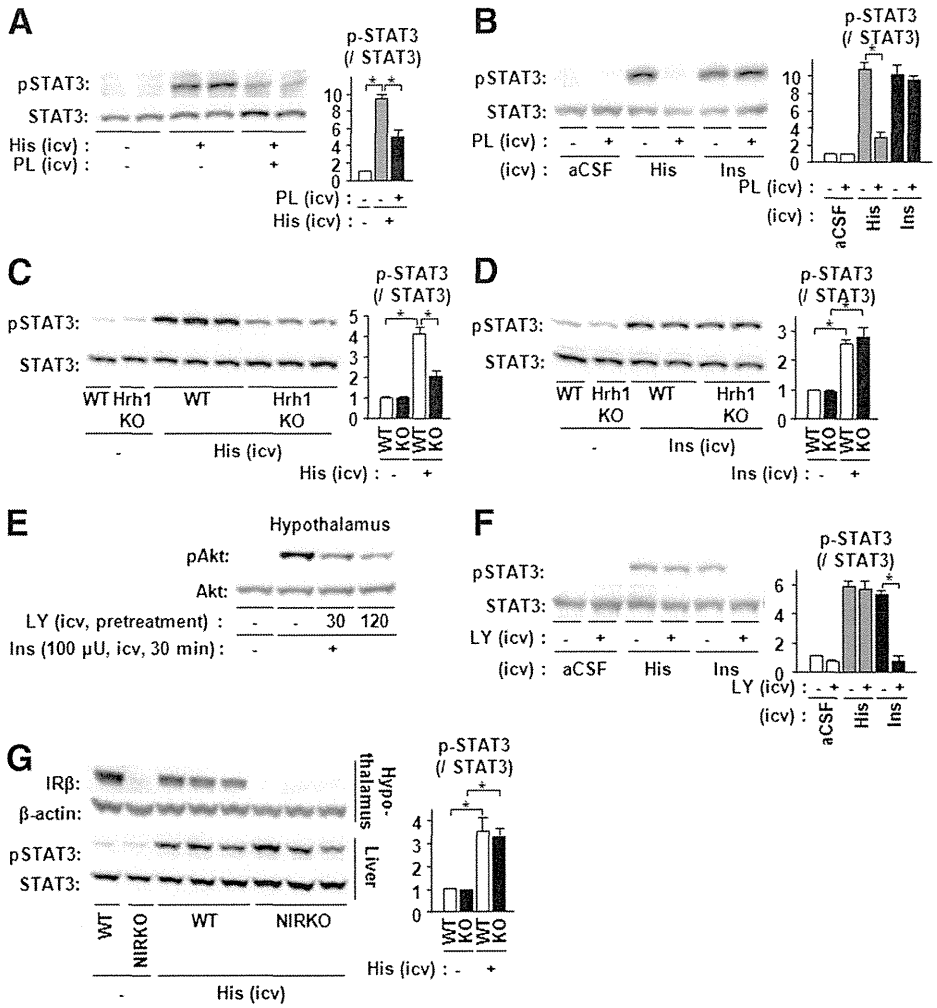

FIG. 8. Central histidine (His) action on the liver is independent of central insulin (Ins) action. *A* **and** *B*: **Phosphorylation of STAT3 was analyzed at 180 min after the intravenous administration of somatostatin (3 μg · kg^{-1} · min^{-1}) and the lateral ventricular administration of histidine (*A* and *B*) or insulin (*B*), which was performed at 15 min after the ICV preadministration of the histamine H_1 antagonist pyrilamine (50 μg/mouse). Quantitation is represented as means ± SE (*n* = 6–8).** *C* **and** *D*: **Somatostatin administration (3 μg · kg^{-1} · min^{-1}) and the lateral ventricular administration of histidine (*C*) or insulin (*D*) were performed in Hrh1KO mice, and the phosphorylation of hepatic STAT3 was analyzed at 180 min postadministration. Quantitation is represented as means ± SE (*n* = 6).** *E*: **The ICV administration of insulin (100 μU/mouse, bolus) was performed at 30 and 120 min after the administration of the PI3-K inhibitor LY294002 (10 nmol/mouse; LY). The phosphorylation of hypothalamic Akt at 30 min after insulin administration is shown.** *F*: **Somatostatin administration (3 μg · kg^{-1} · min^{-1}) and the lateral ventricular administration of histidine or insulin were performed at 120 min after the lateral ventricular administration of LY294002 (10 nmol/mouse; LY), and the phosphorylation of hepatic STAT3 was analyzed at 180 min postadministration. Quantitation is represented as means ± SE (*n* = 5).** *G*: **Somatostatin (3 μg · kg^{-1} · min^{-1}) and histidine were administered into NIRKO mice, and the levels of hypothalamic insulin receptor (IRβ), β-actin, and hepatic STAT3 were analyzed at 180 min postadministration. Quantitation is represented as means ± SE (*n* = 6). aCSF, artificial cerebrospinal fluid; WT, wild type.**

Insulin-dependent phosphorylation of hypothalamic Akt was attenuated by the ICV administration of the PI3-K inhibitor LY294002 (Fig. 8*E*). We therefore investigated the effect of the ICV administration of histidine or insulin, with the concurrent administration of LY294002, on the phosphorylation of hepatic STAT3. LY294002 inhibited the insulin-induced phosphorylation of hepatic STAT3 but did not affect its phosphorylation by histidine (Fig. 8*F*). We also examined mice lacking central insulin receptors. In the NIRKO mice, as in the control mice, the ICV administration of histidine induced hepatic STAT3 phosphorylation (Fig. 8*G*). These results suggest that central histidine action mediated by the histamine H_1 receptor is independent of central insulin action but that they function additively to suppress HGP.

DISCUSSION

The central nervous system monitors hormonal and nutritional changes that regulate energy metabolism in peripheral tissues. In this study, we revealed that an increase in blood histidine levels acts on the central nervous system, activates hepatic IL-6/STAT3 signaling, suppresses the expression of gluconeogenic genes in the liver, and augments the insulin-dependent suppression of HGP. These findings suggest that histidine can be a target molecule for the treatment of type 2 diabetes. Recently, plasma histidine levels were reported to show a significant inverse association with fasting and 2-h blood glucose levels during glucose tolerance tests in individuals without diabetes or newly diagnosed male patients with type 2 diabetes (14). Histidine was also shown to improve the hyperglycemia induced by

the central administration of 2-deoxyglucose in rodents (26); however, the mechanism by which histidine lowers blood glucose levels is not clear. In the current study, the intraperitoneal administration of histidine induced the phosphorylation of hepatic STAT3 and reduced blood glucose levels associated with glucose loading. Consistent with a previous study showing that histidine is not involved in the secretion of insulin (27), histidine did not significantly affect plasma insulin levels in the current study. In the hyperinsulinemic-euglycemic clamp experiment, the intravenous administration of histidine increased GIR and the suppression of HGP. Such histidine action was not observed in LST3KO mice or Kupffer cell–depleted mice, suggesting that the activation of hepatic IL-6/STAT3 signaling plays an important role in the histidine-mediated suppression of HGP. The gene expression of *G6pc* and *Pck1* was downregulated by histidine administration in the hyperinsulinemic-euglycemic clamp experiment, with a clear reduction in the protein levels of G6Pase but not PEPCK. These findings suggest that the downregulation of G6Pase expression causes the suppression of HGP by histidine. However, the activation of hepatic STAT3 by histidine alone is relatively weak, resulting in the mild suppression of *G6pc* gene expression but not of *Pck1*. Furthermore, euglycemic-pancreatic clamp tests with histidine did not reveal a significant change in HGP. These findings may explain why histidine administration alone is not enough to affect the homeostasis of blood glucose levels.

In the brain, histidine is converted into histamine by histidine decarboxylase in the tuberomammillary nucleus of the posterior hypothalamus (24,25,28). Consistent with a previous study (25), hypothalamic histamine content was increased by histidine administration in the current study. A previous study using rats showed that enhanced central histamine action due to histidine administration suppresses food intake (25). In contrast, both Hrh1KO mice (29) and histidine decarboxylase knockout mice (30) present with insulin resistance as well as obesity. In addition, the development of obesity and diabetes caused by the antipsychotic drug olanzapine in humans is reportedly linked to inhibition of the histamine H_1 receptor (31). Such phenotypes may indicate that the action of histamine affects not only food intake but also glucose metabolism. In this study, the central administration of histamine H_1 receptor antagonist attenuated the activation of hepatic STAT3 and the suppression of HGP induced by the systemic administration of histidine. Furthermore, the central administration of histidine also activated hepatic STAT3 while suppressing HGP. These findings indicate that the histidine-induced suppression of HGP, as well as the suppression of food intake, is mediated by central histamine action. Because the histamine-containing neurons in the tuberomammillary nucleus project into most of the brain (28), the precise mechanism in the brain by which central histamine activates hepatic STAT3 remains unclear. This histidine action is additive to the insulin-induced suppression of HGP. The activation of hepatic STAT3 by central insulin action was not blocked by the central administration of a histamine H_1 receptor antagonist or in Hrh1KO mice. In contrast, the activation of hepatic STAT3 by central histidine was not blocked by the central administration of a PI3-K inhibitor or in NIRKO mice, suggesting that the mechanism underlying the action of central histidine is independent of insulin action.

This study demonstrates that the activation of hepatic IL-6/STAT3 signaling pathways and downregulation of hepatic gluconeogenic gene expression by histidine are mediated by central histamine action involving the histamine H_1 receptor. Central histidine action, which has a central nervous system mechanism that is independent of insulin, augments the insulin-dependent suppression of glucose production in the liver. This study indicates that the central mechanism by which histidine regulates hepatic glucose metabolism and activates hepatic STAT3 is a potential target for the treatment of type 2 diabetic patients with elevated gluconeogenesis.

ACKNOWLEDGMENTS

This work was supported by the Program for Promotion of Basic and Applied Research for Innovations in Bio-oriented Industry to H.I.; Ministry of Education, Culture, Sports, Science and Technology MEXT KAKENHI Grant 23126509 to H.I.; and Japan Society for the Promotion of Science KAKENHI grants 23300274 to H.I. and 24790919 to K.K.

ThinkSCIENCE, Inc. (Tokyo, Japan), assisted with manuscript preparation. No other potential conflicts of interest relevant to this article were reported.

K.K., Y.N., Y.I., S.As., T.M., H.W., A.M., and F.I. produced the data. M.M., T.O., and H.N. produced the data and contributed to the discussion. Y.K., C.M., K.T., S.Ak., and S.K. contributed to the discussion. M.K. contributed to the discussion and reviewed and edited the manuscript. H.I. researched the data, designed the study, contributed to the discussion, and wrote the manuscript. H.I. is the guarantor of this work and, as such, had full access to all the data in the study and takes responsibility for the integrity of the data and the accuracy of the data analysis.

The authors thank C.R. Kahn (Harvard Medical School) for NIRKO mice; H. Nakamura (Kanazawa University) for expert advice on the statistical analysis; and Y. Anraku, M. Nishio, and C. Asahi (Kanazawa University) for technical assistance.

REFERENCES

1. Magnusson I, Rothman DL, Katz LD, Shulman RG, Shulman GI. Increased rate of gluconeogenesis in type II diabetes mellitus. A ^{13}C nuclear magnetic resonance study. J Clin Invest 1992;90:1323–1327
2. Radziuk J, Pye S. Hepatic glucose uptake, gluconeogenesis and the regulation of glycogen synthesis. Diabetes Metab Res Rev 2001;17:250–272
3. Dentin R, Hedrick S, Xie J, Yates J 3rd, Montminy M. Hepatic glucose sensing via the CREB coactivator CRTC2. Science 2008;319:1402–1405
4. Rodgers JT, Haas W, Gygi SP, Puigserver P. Cdc2-like kinase 2 is an insulin-regulated suppressor of hepatic gluconeogenesis. Cell Metab 2010;11:23–34
5. Inoue H, Ogawa W, Ozaki M, et al. Role of STAT-3 in regulation of hepatic gluconeogenic genes and carbohydrate metabolism in vivo. Nat Med 2004;10:168–174
6. Kimura K, Yamada T, Matsumoto M, et al. Endoplasmic reticulum stress inhibits STAT3-dependent suppression of hepatic gluconeogenesis via dephosphorylation and deacetylation. Diabetes 2012;61:61–73
7. Lam TK. Neuronal regulation of homeostasis by nutrient sensing. Nat Med 2010;16:392–395
8. Cota D, Proulx K, Seeley RJ. The role of CNS fuel sensing in energy and glucose regulation. Gastroenterology 2007;132:2158–2168
9. Inoue H, Ogawa W, Asakawa A, et al. Role of hepatic STAT3 in brain-insulin action on hepatic glucose production. Cell Metab 2006;3:267–275
10. Obici S, Zhang BB, Karkanias G, Rossetti L. Hypothalamic insulin signaling is required for inhibition of glucose production. Nat Med 2002;8:1376–1382
11. Pocai A, Obici S, Schwartz GJ, Rossetti L. A brain-liver circuit regulates glucose homeostasis. Cell Metab 2005;1:53–61
12. Lam TK, Gutierrez-Juarez R, Pocai A, Rossetti L. Regulation of blood glucose by hypothalamic pyruvate metabolism. Science 2005;309:943–947

13. Obici S, Feng Z, Morgan K, Stein D, Karkanias G, Rossetti L. Central administration of oleic acid inhibits glucose production and food intake. Diabetes 2002;51:271–275
14. Stancáková A, Civelek M, Saleem NK, et al. Hyperglycemia and a common variant of GCKR are associated with the levels of eight amino acids in 9,369 Finnish men. Diabetes 2012;61:1895–1902
15. Su Y, Lam TK, He W, et al. Hypothalamic leucine metabolism regulates liver glucose production. Diabetes 2012;61:85–93
16. Inoue I, Yanai K, Kitamura D, et al. Impaired locomotor activity and exploratory behavior in mice lacking histamine H1 receptors. Proc Natl Acad Sci USA 1996;93:13316–13320
17. Brüning JC, Gautam D, Burks DJ, et al. Role of brain insulin receptor in control of body weight and reproduction. Science 2000;289:2122–2125
18. Nuttall FQ, Mooradian AD, Gannon MC, Billington C, Krezowski P. Effect of protein ingestion on the glucose and insulin response to a standardized oral glucose load. Diabetes Care 1984;7:465–470
19. Semon BA, Leung PM, Rogers QR, Gietzen DW. Increase in plasma ammonia and amino acids when rats are fed a 44% casein diet. Physiol Behav 1988;43:631–636
20. Miyake K, Ogawa W, Matsumoto M, Nakamura T, Sakaue H, Kasuga M. Hyperinsulinemia, glucose intolerance, and dyslipidemia induced by acute inhibition of phosphoinositide 3-kinase signaling in the liver. J Clin Invest 2002;110:1483–1491
21. Kyriazis GA, Soundarapandian MM, Tyrberg B. Sweet taste receptor signaling in beta cells mediates fructose-induced potentiation of glucose-stimulated insulin secretion. Proc Natl Acad Sci USA 2012;109: E524–E532
22. Van Rooijen N, Sanders A. Kupffer cell depletion by liposome-delivered drugs: comparative activity of intracellular clodronate, propamidine, and ethylenediaminetetraacetic acid. Hepatology 1996;23:1239–1243
23. Salkowski CA, Neta R, Wynn TA, Strassmann G, van Rooijen N, Vogel SN. Effect of liposome-mediated macrophage depletion on LPS-induced cytokine gene expression and radioprotection. J Immunol 1995;155:3168–3179
24. Anderson GH. Diet, neurotransmitters and brain function. Br Med Bull 1981;37:95–100
25. Yoshimatsu H, Chiba S, Tajima D, Akehi Y, Sakata T. Histidine suppresses food intake through its conversion into neuronal histamine. Exp Biol Med (Maywood) 2002;227:63–68
26. Nagai K, Niijima A, Yamano T, et al. Possible role of L-carnosine in the regulation of blood glucose through controlling autonomic nerves. Exp Biol Med (Maywood) 2003;228:1138–1145
27. Floyd JC Jr, Fajans SS, Conn JW, Knopf RF, Rull J. Stimulation of insulin secretion by amino acids. J Clin Invest 1966;45:1487–1502
28. Haas H, Panula P. The role of histamine and the tuberomamillary nucleus in the nervous system. Nat Rev Neurosci 2003;4:121–130
29. Masaki T, Chiba S, Yasuda T, et al. Involvement of hypothalamic histamine H1 receptor in the regulation of feeding rhythm and obesity. Diabetes 2004; 53:2250–2260
30. Fülöp AK, Földes A, Buzás E, et al. Hyperleptinemia, visceral adiposity, and decreased glucose tolerance in mice with a targeted disruption of the histidine decarboxylase gene. Endocrinology 2003;144:4306–4314
31. Deng C, Weston-Green K, Huang XF. The role of histaminergic H1 and H3 receptors in food intake: a mechanism for atypical antipsychotic-induced weight gain? Prog Neuropsychopharmacol Biol Psychiatry 2010;34:1–4

JVI
Journals.ASM.org

MicroRNA-27a Regulates Lipid Metabolism and Inhibits Hepatitis C Virus Replication in Human Hepatoma Cells

Takayoshi Shirasaki,[a,b] Masao Honda,[a,b] Tetsuro Shimakami,[a] Rika Horii,[a] Taro Yamashita,[a] Yoshio Sakai,[a] Akito Sakai,[a] Hikari Okada,[a] Risa Watanabe,[b] Seishi Murakami,[a] MinKyung Yi,[c] Stanley M. Lemon,[d] Shuichi Kaneko[a]

Department of Gastroenterology, Kanazawa University Graduate School of Medical Science, Kanazawa, Japan[a]; Department of Advanced Medical Technology, Kanazawa University Graduate School of Health Medicine, Kanazawa, Japan[b]; Human Center for Hepatitis Research, Institute for Human Infections and Immunity, and Department of Microbiology and Immunology, University of Texas Medical Branch, Galveston, Texas, USA[c]; Division of Infectious Diseases, School of Medicine, The University of North Carolina at Chapel Hill, Chapel Hill, North Carolina, USA[d]

The replication and infectivity of the lipotropic hepatitis C virus (HCV) are regulated by cellular lipid status. Among differentially expressed microRNAs (miRNAs), we found that miR-27a was preferentially expressed in HCV-infected liver over hepatitis B virus (HBV)-infected liver. Gene expression profiling of Huh-7.5 cells showed that miR-27a regulates lipid metabolism by targeting the lipid synthetic transcription factor RXRα and the lipid transporter ATP-binding cassette subfamily A member 1. In addition, miR-27a repressed the expression of many lipid metabolism-related genes, including *FASN*, *SREBP1*, *SREBP2*, *PPARα*, and *PPARγ*, as well as *ApoA1*, *ApoB100*, and *ApoE3*, which are essential for the production of infectious viral particles. miR-27a repression increased the cellular lipid content, decreased the buoyant density of HCV particles from 1.13 to 1.08 g/cm^3, and increased viral replication and infectivity. miR-27a overexpression substantially decreased viral infectivity. Furthermore, miR-27a enhanced *in vitro* interferon (IFN) signaling, and patients who expressed high levels of miR-27a in the liver showed a more favorable response to pegylated IFN and ribavirin combination therapy. Interestingly, the expression of miR-27a was upregulated by HCV infection and lipid overload through the adipocyte differentiation transcription factor C/EBPα. In turn, upregulated miR-27a repressed HCV infection and lipid storage in cells. Thus, this negative feedback mechanism might contribute to the maintenance of a low viral load and would be beneficial to the virus by allowing it to escape host immune surveillance and establish a persistent chronic HCV infection.

MicroRNA (miRNA) is a small, endogenous, single-stranded, noncoding RNA consisting of 20 to 25 bases that regulates gene expression. It plays an important role in various biological processes, including organ development, differentiation, and cellular death and proliferation, and is also involved in infection and diseases such as cancer (1).

Previously, we examined miRNA expression in hepatocellular carcinoma (HCC) and noncancerous background liver tissue infected with hepatitis B virus (HBV) and HCV (2). We showed that some miRNAs were differentially expressed according to HBV or HCV infection but not according to the presence of HCC. These infection-specific miRNAs were believed to regulate HBV or HCV replication; however, their functional role has not been elucidated.

HCV is described as a lipotropic virus because of its association with serum lipoprotein (3–5). It utilizes the low-density lipoprotein (LDL) receptor for cellular entry (6–8) and forms replication complexes on lipid rafts (9). The HCV core protein surrounds and binds lipid droplets (LDs) and nonstructural proteins on the endoplasmic reticulum (ER) membrane, which is essential for particle formation (10). Moreover, HCV cellular secretion is linked to very LDL (VLDL) secretion (11). In liver tissue histology, steatosis is often observed in chronic hepatitis C (CH-C) and is closely related to resistance to interferon (IFN) treatment (12, 13). Thus, lipids play important roles in HCV replication and CH-C pathogenesis.

Several miRNAs, such as miR-122 (14), miR-199a (15), miR-196 (16), miR-29 (17), Let-7b (18), and miR-130a (19), reportedly regulate HCV replication; however, miRNAs that regulate lipid metabolism and HCV replication have not been reported so far. Previously, we reported that 19 miRNAs were differentially expressed in HBV- and HCV-infected livers (2). In the present study, we evaluated the functional relevance of miR-27a in HCV replication by using the human hepatoma cell line Huh-7.5. We analyzed the regulation of lipid metabolism by miR-27a in hepatocytes and revealed a unique pathophysiological relationship between lipid metabolism and HCV replication in CH-C.

MATERIALS AND METHODS

Cell line. Huh-7.5 cells (kindly provided by C. M. Rice, Rockefeller University, New York, NY) were maintained in Dulbecco's modified Eagle's medium (DMEM; Gibco BRL, Gaithersburg, MD) containing 10% fetal bovine serum (FBS) and 1% penicillin-streptomycin.

HCV replication analysis. HCV replication analysis was performed by transfecting Huh-7.5 cells with JFH-1 (20), H77Sv2 Gluc2A (21), and their derivative RNA constructs. pH77Sv2 is a modification of pH77S, a plasmid containing the full-length sequence of the genotype 1a H77 HCV strain with five cell culture-adaptive mutations that promote its replication in Huh-7 hepatoma cells (21–24). pH77Sv2 Gluc2A is a related construct in which the *Gaussia* luciferase (Gluc) sequence, fused to the 2A autocatalytic protease of foot-and-mouth virus RNA, was inserted in frame between p7 and NS2 (21, 23, 25). pH77Sv2 Gluc2A (AAG) is a control plasmid that has an NS5B polymerase catalytic domain mutation.

Received 29 October 2012 Accepted 21 February 2013
Published ahead of print 28 February 2013
Address correspondence to Masao Honda, mhonda@m-kanazawa.jp.

doi:10.1128/JVI.03022-12

For RNA transfection, the cells were washed with phosphate-buffered saline (PBS) and resuspended in complete growth medium. The cells were then pelleted by centrifugation (1,400 × *g* for 4 min at 4°C), washed twice with ice-cold PBS, and resuspended in ice-cold PBS at a concentration of 7.5×10^6 cells/0.4 ml. The cells were mixed with 10 μg of the RNA transcripts, placed into 2-mm-gap electroporation cuvettes (BTX Genetronics, San Diego, CA), and electroporated with five pulses of 99 μs at 750 V over 1.1 s in an ECM 830 (BTX Genetronics). Following a 10-min recovery period, the cells were mixed with complete growth medium and plated.

miR-27a and anti-miR-27a transfection. Huh-7.5 cells transfected with pH77Sv2 Gluc2A RNA or pH77Sv2 Gluc2A (AAG) RNA were transfected with 50 nM synthetic miRNA (pre-miRNA) or 50 nM anti-miRNA (Ambion Inc., Austin, TX) with the siPORTTM NeoFXTM Transfection Agent (Ambion). Transfection was performed immediately by mixing the electroporated cells with the miRNA transfection reagents. Control samples were transfected with an equal concentration of a nontargeting control (pre-miRNA negative control) or inhibitor negative control (anti-miRNA negative control) to assess non-sequence-specific effects in the miRNA experiments.

Fatty acid treatment. Huh-7.5 cells transfected with HCV RNA and pre- or anti-miRNA were cultured for 24 h and then treated with the indicated concentrations of oleic acid (0 to 250 μM) (26) in the presence of 2% free fatty acid (FFA)-free bovine serum albumin (BSA; Sigma-Aldrich, St. Louis, MO). The cells were harvested at 72 h posttreatment with oleic acid for quantitative real-time detection PCR (RTD-PCR), Western blotting, immunofluorescence staining, and reporter analysis. The number of viable cells was determined by an MTS assay [one-step 3-(4,5-dimethylthiazol-2-yl)-2,5-diphenyltetrazolium bromide assay; Promega Corporation, Madison, WI]. Cellular triglyceride (TG) and cholesterol (TCHO) contents were measured with TG Test Wako and Cholesterol Test Wako kits (Wako, Osaka, Japan) according to the manufacturer's instructions.

Equilibrium ultracentrifugation of JFH-1 particles in isopycnic iodixanol gradients. Filtered supernatant fluids collected from JFH-1 RNA- and pre-miRNA- or anti-miRNA-transfected cell cultures were concentrated 30-fold with a Centricon PBHK Centrifugal Plus-20 filter unit with an Ultracel PL membrane (100-kDa exclusion; Merck Millipore, Billerica, MA) and then layered on top of a preformed continuous 10 to 40% iodixanol (OptiPrep; Sigma-Aldrich) gradient in Hanks' balanced salt solution (Invitrogen, Carlsbad, CA) as described previously (24). The gradients were centrifuged in an SW41 rotor (Beckman Coulter Inc., Brea, CA) at 35,000 rpm for 16 h at 4°C, and the fractions (500 μl each) were collected from the top of the tube. The density of each fraction was determined with a digital refractometer (Atago, Tokyo, Japan).

Infectivity assays. Huh-7.5 cells were seeded at 5.0×10^4/well in 48-well plates 24 h before inoculation with 100 μl of the gradient fractions. The cells were tested for the presence of intracellular core antigen by immunofluorescence 72 h later, as described below. Clusters of infected cells that stained for the core antigen were considered to constitute a single infectious focus, and virus titers were calculated accordingly in terms of numbers of focus-forming units (FFU)/ml.

Western blotting and immunofluorescence staining. Western blotting was performed as described previously (27). The cells were washed in PBS and lysed in radioimmunoprecipitation assay buffer containing Complete protease inhibitor cocktail and PhosSTOP (Roche Applied Science, Indianapolis, IN). The membranes were blocked in Blocking One or Blocking One-P solution (Nacalai Tesque, Kyoto, Japan), and the expression of HCV core protein, retinoid X receptor alpha (RXRα), sterol regulatory element-binding protein (SREBP1), ATP-binding cassette subfamily A member 1 (ABCA1), ApoE3, ApoB100, fatty acid synthase (FASN), peroxisome proliferator-activated receptor α (PPARα), ApoA1, phospho-PKR-like ER kinase (phospho-PERK), PERK, phospho-eIF2α, eIF2α, BIP, phospho-STAT1, and β-actin was evaluated with mouse anti-core (Thermo Fisher Scientific Inc., Rockford, IL), rabbit anti-RXRα, rabbit anti-SREBP1 (Santa Cruz Biotechnology Inc., Santa Cruz, CA), mouse anti-ABCA1 (Abcam, Cambridge, MA), goat anti-ApoE3, goat anti-ApoB100 (R&D Systems Inc., Minneapolis, MN), rabbit anti-FASN, rabbit anti-PPARα, mouse anti-ApoA1, rabbit anti-phospho-PERK, rabbit anti-PERK, rabbit anti-phospho-eIF2α, rabbit anti-eIF2α, rabbit anti-BIP, rabbit anti-phospho-STAT1, and rabbit anti-β-actin antibodies (Cell Signaling Technology Inc., Danvers, MA), respectively.

For immunofluorescence staining, the cells were washed twice with PBS and fixed in 4% paraformaldehyde for 15 min at room temperature. After washing again with PBS, the cells were permeabilized with 0.05% Triton X-100 in PBS for 15 min at room temperature. They were then incubated in a blocking solution (10% FBS and 5% BSA in PBS) for 30 min and with the anti-core monoclonal antibodies. The fluorescent secondary antibodies were Alexa 568-conjugated anti-mouse IgG antibodies (Invitrogen). Nuclei were labeled with 4′,6-diamidino-2-phenylindole (DAPI), and LDs were visualized with boron-dipyrromethene (BODIPY) 493/503 (Invitrogen). Imaging was performed with a CSU-X1 confocal microscope (Yokogawa Electric Corporation, Tokyo, Japan).

Quantitative RTD-PCR. Total RNA was isolated with a GenElute Mammalian Total RNA Miniprep kit (Sigma-Aldrich), and cDNA was synthesized with a high-capacity cDNA reverse transcription kit (Applied Biosystems, Carlsbad, CA). The primer pairs and probes for C/EBPα, ABCA1, PPARγ, SREBF1, SREBF2, FASN, 2′-5′-oligoadenylate synthetase 2 (OAS2), and β-actin were obtained from the TaqMan assay reagent library. HCV RNA was detected as described previously (28). HCV RNA was isolated from viral particles with a QIAamp viral RNA kit (Qiagen, Inc., Valencia, CA) in accordance with the manufacturer's instructions. Total RNA containing miRNA was isolated according to the protocol of the mirVana miRNA isolation kit (Ambion). For the enrichment of mature miRNA, argonaute 2 (Ago2)-binding miRNA was immunoprecipitated with an anti-Ago2 monoclonal antibody (Wako) and mature miRNA was eluted from the precipitant with a microRNA isolation kit, Human Ago2 (Wako). cDNA was prepared via reverse transcription with 10 ng of isolated total RNA and 3 μl of each reverse transcription primer with specific loop structures. Reverse transcription was performed with a TaqMan MicroRNA reverse transcription kit (Applied Biosystems) according to the manufacturer's protocol. RTD-PCR was performed with the 7500 Real Time PCR system (Applied Biosystems) according to the manufacturer's instructions. The primer pairs and probes for miR-let7a, miR-34c, miR-142-5p, miR-27a, miR-23a, and RNU6B were obtained from the TaqMan assay reagent library.

3′ UTR luciferase reporter assays. The miRNA expression reporter vector pmirGLO Dual-Luciferase miRNA Target Expression Vector (Promega Corporation) was used to validate the RXRα and ABCA1 3′ untranslated regions (UTRs) as miRNA binding sites. cDNA fragments corresponding to the entire 3′ UTR of human RXRα and human ABCA1 were amplified with the Access RT-PCR system (Promega Corporation) from total RNA extracted from Huh-7.5 cells. The PCR products were cloned into the designated multiple cloning site downstream of the luciferase open reading frame between the SacI and XhoI restriction sites of the pCR2.1-TOPO vector (Invitrogen). Point mutations in the seed region of the predicted miR-27a sites within the 3′ UTR of human RXRα and human ABCA1 were generated with a QuikChange Multi site-directed mutagenesis kit (Agilent Technologies Inc., Santa Clara, CA) according to the manufacturer's protocol. All constructs were confirmed by sequencing.

Huh-7.5 cells were grown to 70% confluence in 24-well plates in complete DMEM. The cells were cotransfected with 200 ng of the indicated 3′ UTR luciferase reporter vector and 50 nM synthetic miRNA (pre-miRNA) or 50 nM anti-miRNA (Ambion) in a final volume of 0.5 ml with Lipofectamine 2000 (Invitrogen). At 24 h posttransfection, firefly and *Renilla* luciferase activities were measured consecutively with the Dual-Luciferase Reporter Assay system (Promega Corporation).

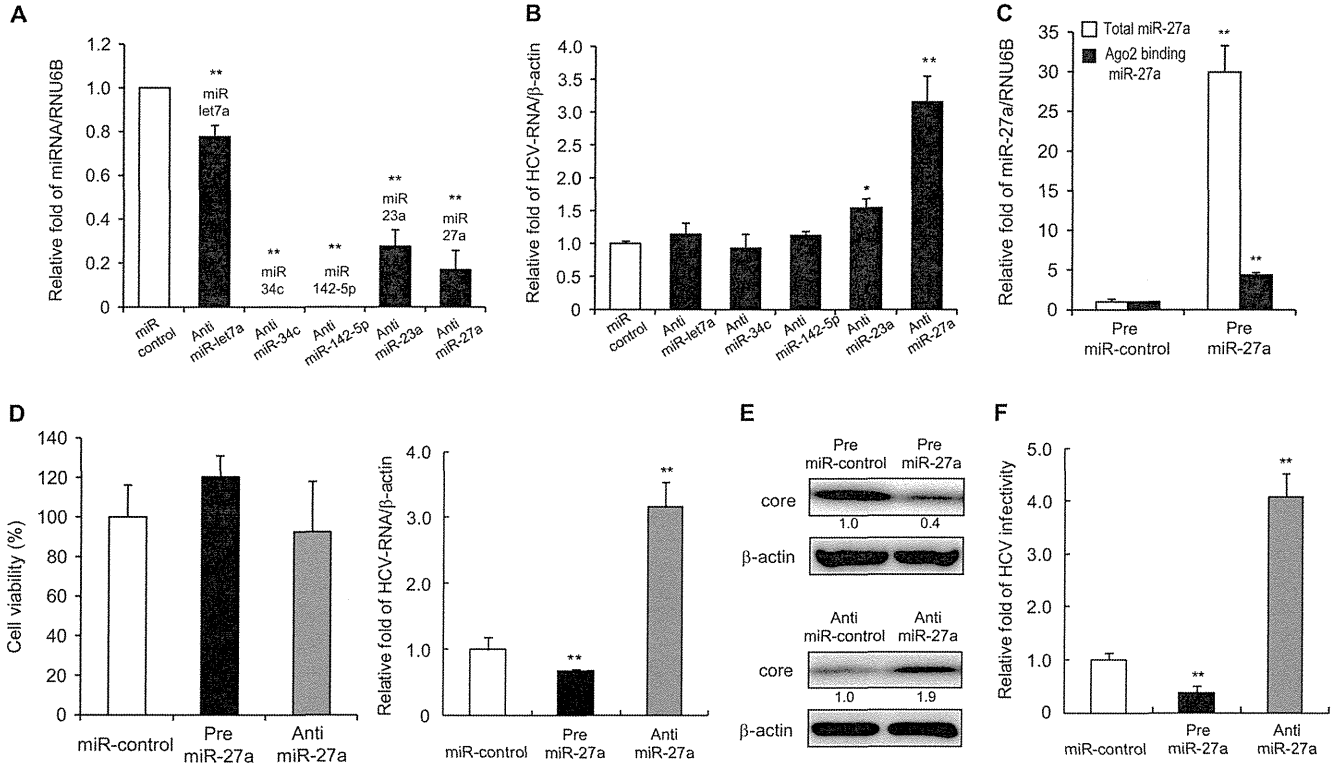

FIG 1 miR-27a has a negative effect on HCV replication and infectivity. Huh-7.5 cells were transfected with JFH-1 RNA and pre- or anti-miRNA. Expression was quantified at 72 h posttransfection. (A) Inhibition efficiency of miRNAs by anti-miRNAs (RTD-PCR, $n = 6$). (B) Effects of anti-miRNAs on HCV replication (RTD-PCR, $n = 6$). (C) Detection of whole miR-27a and Ago2-binding miR-27a in Huh-7.5 cells. At 72 h posttransfection, cells were harvested and Ago2-binding miRNA was purified as described in Materials and Methods. White bars indicate total miR-27a levels, and black bars indicate Ago2-binding miR-27a levels (RTD-PCR, $n = 6$). (D) Effects of pre- or anti-miR-27a on cell viability (left) and HCV replication (right). Cell viability (%) was assessed by the MTS assay ($n = 6$). (E) Effects of pre- or anti-miR-27a on HCV core protein levels by Western blotting. (F) Effects of pre- or anti-miR-27a on HCV infection. Huh-7.5 cells were infected with HCVcc derived from Huh-7.5 cells transfected with pre- or anti-miR-27a and JFH-1 RNA. HCV RNA was quantified at 72 h postinfection by RTD-PCR ($n = 6$). All experiments were performed in duplicate and repeated three times. Values are means ± standard errors. *, $P < 0.01$; **, $P < 0.005$.

Promoter analysis. DNA fragments from −400 to +36 bp and from −700 to +36 bp relative to the transcription initiation site of pri-miR-23a~27a~24-2 were inserted into pGL3-Basic (Promega Corporation) at the MluI and XhoI sites. Point mutations in the seed region of predicted C/EBPα binding sites were generated with a QuikChange Multi site-directed mutagenesis kit (Agilent Technologies) according to the manufacturer's protocol. All constructs were confirmed by sequencing.

Huh-7.5 cells transfected with HCV RNA were cultured for 24 h in 24-well plates, and then 200 ng of the plasmids was cotransfected with 2 ng of the *Renilla* luciferase expression vector (pSV40-Renilla) with the FuGENE6 Transfection Reagent (Roche Applied Science). After 24 h, the cells were treated with oleic acid in the presence of 2% FFA-free BSA (Sigma-Aldrich). At 48 h posttreatment, a luciferase assay was carried out with the Dual-Luciferase Reporter Assay system (Promega Corporation) according to the manufacturer's instructions.

For tunicamycin treatment, the plasmids (200 ng) were cotransfected with 2 ng pSV40-Renilla with FuGENE6 (Roche Applied Science) into Huh-7.5 cells grown in the wells of 24-well plates. After 24 h, the cells were treated for a further 24 h with the indicated concentrations of tunicamycin and a luciferase assay was carried out as described above.

RNA interference. A small interfering RNA (siRNA) specific to ABCA1 and a control siRNA were obtained from Thermo Fisher Scientific. Transfection was performed with Lipofectamine 2000 (Invitrogen) according to the manufacturer's instructions.

IFN treatment. Huh-7.5 cells transfected with HCV RNA and pre- or anti-miRNA were treated with oleic acid as described above. At 48 h later, the cells were treated with the indicated number of international units of IFN-α for 24 h.

Affymetrix GeneChip analysis. Aliquots of total RNA (50 ng) isolated from the cells were subjected to amplification with the WT-Ovation Pico RNA Amplification system (NuGen, San Carlos, CA) according to the manufacturer's instructions. The Affymetrix Human U133 Plus 2.0 microarray chip containing 54,675 probes has been described previously (29).

Statistical analysis. Results are expressed as mean values ± standard errors. At least six samples were tested in each assay. Significance was tested by one-way analysis of variance with Bonferroni methods, and differences were considered statistically significant at P values of <0.01 (*, $P < 0.01$; **, $P < 0.005$).

Microarray accession number. The expression data determined in this study were deposited in the Gene Expression Omnibus database (NCBI) under accession number GSE41737.

RESULTS

Functional relevance of the upregulated miRNAs in HCV-infected livers. Previously, 19 miRNAs were shown to be differentially expressed in HBV- and HCV-infected livers (2). Of these, 6 miRNAs were upregulated and 13 were downregulated. In this study, we focused on the upregulated miRNAs, as they might play a positive role in HCV replication. Anti-miRNAs and the control miRNA were transfected into Huh-7.5 cells following JFH-1 RNA

TABLE 1 Gene categories and names of differentially expressed genes regulated by miR-27a in Huh-7.5 cells

Protein function and name	Gene	Affy ID[a]	GB acc. no.[b]	Fold change		
				Pre-miR-27a/ miR-control	Anti-miR-27a/ anti-miR-control	Pre-miR-27a/ anti-miR-27a
Cytoskeleton remodeling and Wnt signaling						
Collagen, type IV, alpha 6	*COL4A6*	211473_s_at	U04845	0.85	2.19	2.58
Fibronectin 1	*FN1*	214702_at	AJ276395	0.57	1.14	2.02
Filamin A, alpha	*FLNA*	214752_x_at	AI625550	0.64	1.68	2.61
LIM domain kinase 1	*LIMK1*	204357_s_at	NM_002314	0.67	1.63	2.43
p21/Cdc42/Rac1-activated kinase 1	*PAK1*	230100_x_at	AU147145	0.63	1.58	2.53
Breast cancer anti-estrogen resistance 1	*BCAR1*	232442_at	AU147442	0.96	1.94	2.01
Frizzled homolog 3 (*Drosophila*)	*FZD3*	219683_at	NM_017412	0.51	1.30	2.55
Laminin, alpha 4	*LAMA4*	210990_s_at	U77706	0.63	1.26	2.00
Regulation of lipid metabolism						
CREB binding protein (Rubinstein-Taybi syndrome)	*CREBBP*	235858_at	BF507909	0.54	1.50	2.76
NF-Y	*NF-Y*	228431_at	AL137443	0.41	1.44	3.50
Sterol regulatory element binding transcription factor 2	*SREBF2*	242748_at	AA112403	0.47	1.11	2.35
Membrane-bound transcription factor peptidase, site 2	*MBTPS2*	1554604_at	BC036465	0.50	1.21	2.39
Adenosine A2A receptor signaling						
Mitogen-activated protein kinase kinase 7	*MAP2K7*	226053_at	AI090153	0.90	2.07	2.31
Par-6 partitioning defective 6 homolog beta	*PARD6B*	235165_at	AW151704	0.56	1.35	2.43
Rap guanine nucleotide exchange factor (GEF) 2	*RAPGEF2*	238176_at	T86196	0.46	1.36	2.98
Ribosomal protein S6 kinase, 90kDa, polypeptide 2	*RPS6KA2*	204906_at	BC002363	0.61	1.72	2.83
p53 regulation						
MDM2	*MDM2*	237891_at	AI274906	0.41	1.27	3.07
Ubiquitin B	*UBB*	217144_at	X04801	0.58	1.89	3.24
Promyelocytic leukemia	*PML*	235508_at	AW291023	0.52	1.45	2.80
SMT3 suppressor of mif two 3 homolog 1	*SUMO1*	208762_at	U83117	0.55	1.23	2.22
IL-8 in angiogenesis						
B-cell CLL/lymphoma 10	*BCL10*	1557257_at	AA994334	0.59	1.23	2.08
Janus kinase 2	*JAK2*	205841_at	NM_004972	0.77	1.71	2.23
Sphingosine-1-phosphate receptor 1						
G protein, alpha inhibiting activity polypeptide 2	*GNAI2*	201040_at	NM_002070	0.69	1.49	2.15
G protein, beta polypeptide 4	*GNB4*	223487_x_at	AW504458	0.86	1.78	2.06
Mitogen-activated protein kinase 1	*MAPK1*	1552263_at	NM_138957	0.87	1.93	2.22
GRB2-associated binding protein 1	*GAB1*	226002_at	AK022142	0.66	1.40	2.11

[a] Affy ID, Affymetrix identification number.
[b] GB acc. no., GenBank accession number.

transfection. The efficiency with which these anti-miRNAs inhibit the miRNAs is shown in Fig. 1A. Unexpectedly, inhibition of these miRNAs either had no effect or increased HCV replication in the cases of anti-miR-23a and anti-miR-27a (Fig. 1B).

To investigate the functional relevance of miR-27a in HCV replication in more detail, we evaluated JFH-1 replication in Huh-7.5 cells in which miR-27a was inhibited or overexpressed. The efficacy of miR-27a overexpression is shown in Fig. 1C. Although ectopically introduced pre-miR-27a increased miR-27a levels by approximately 30-fold, the levels of endogenous active Ago2 bound to miR-27a in RNA-induced silencing complexes increased by approximately 5-fold. The RNA and core protein levels of JFH-1 in Huh-7.5 cells decreased to 65% and 40%, respectively, following miR-27a overexpression. In contrast, the RNA and core protein levels of JFH-1 increased by 3- and 1.9-fold, respectively, following miR-27a inhibition (Fig. 1D and E). There was no significant difference in cell viability following miR-27a overexpression or inhibition (Fig. 1D). Furthermore, the rate of Huh-7.5 cell infection by JFH-1 decreased to 35% after the overexpression of miR-27a but increased 4-fold after miR-27a inhibition (Fig. 1F). Thus, miR-27a negatively regulates HCV replication and infection.

miR-27a targets the signaling pathways of cytoskeleton remodeling and lipid metabolism in Huh-7.5 cells. We next examined which signaling pathways were modulated by miR-27a. TargetScan (http://www.targetscan.org/) predicts biological targets of miRNAs by searching for the presence of conserved 8- and 7-mer sites that match the seed region of each miRNA (30). A TargetScan (release 5.2) for miR-27a predicted 921 candidate target genes, and functional gene ontology enrichment analysis of these genes by MetaCore (Thomson Reuters, New York, NY) showed that miR-27a could target the cytoskeleton remodeling and lipid metabolism signaling pathways (data not shown).

To examine whether these signaling pathways were regulated by miR-27a, gene expression profiling was carried out with Huh-7.5 cells in which miR-27a was over- or underexpressed. Transfection of cells with pre-miR-27a and pre-miR-

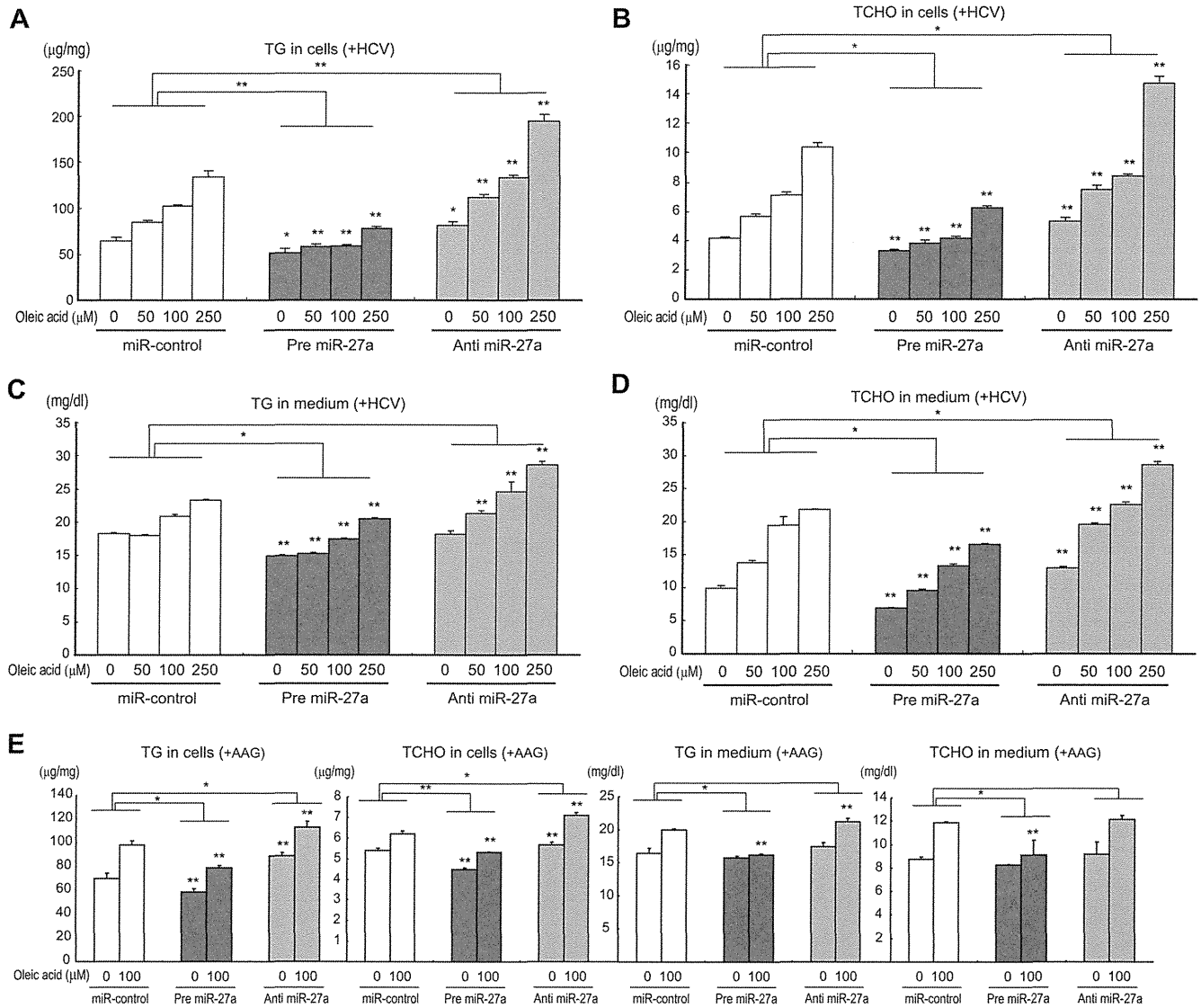

FIG 2 Changes in the lipid contents of Huh-7.5 cells and culture medium caused by pre- and anti-miR-27a. Huh-7.5 cells were transfected with replication-competent HCV RNA (H77Sv2 Gluc2A RNA [+HCV]) or replication-incompetent HCV RNA [H77Sv2 Gluc2A (AAG) (+AAG)] together with pre- or anti-miR-27a. At 24 h posttransfection, increasing amounts of oleic acid (0 to 250 μM) were added to the culture medium, and at 72 h after oleic acid treatment, TG and TCHO levels were measured in the cells and medium. Panels: A, TG in cells; B, TCHO in cells; C, TG in medium; D, TCHO in medium; E, TG and TCHO in cells and medium; A to D, +H77Sv2 Gluc2A (+HCV); E, +H77Sv2 Gluc2A (AAG) (+AAG). Lipid concentration was compared with that of miR-control and pre- or anti-miRNA ($n = 6$). All experiments were performed in duplicate and repeated three times. Values are means ± standard errors. *, $P < 0.01$; **, $P < 0.005$.

control or with anti-miR-27a and anti-miR-control enabled the identification of down- and upregulated genes, respectively. A total of 870 genes were selected with a >2-fold anti-miR-27a/pre-miR-27a expression ratio. Pathway analysis of these genes with MetaCore revealed that they are involved in cytoskeleton remodeling signaling, including that of *COL4A6*, *FN 1*, and *PAK1*; lipid metabolism signaling, including that of *CREBBP* and *SREBF2*; A2A receptor signaling, including that of *RAPGEF2*; and p53 regulation signaling, including that of *MDM2*. These genes were repressed by miR-27a in Huh-7.5 cells (Table 1).

miR-27a reduces TG and TCHO levels in cells and culture medium. Pathway analysis of the gene expression profile regulated by miR-27a in Huh-7.5 cells revealed the presence of many genes involved in lipid metabolism-related signaling pathways. To examine the functional relevance of miR-27a in lipid metabolism, we measured the cellular levels of TG and TCHO in Huh-7.5 cells in which miR-27a was inhibited or overexpressed, respectively. As shown in Fig. 2A and B, TG and TCHO levels in Huh-7.5 cells transfected with miR-control were increased in a dose-dependent manner following the addition of oleic acid (0 to 250 μM). Pre-miR-27a repressed this increase, while anti-miR-27a significantly accelerated it. Similarly, pre-miR-27a repressed the increase in TG and TCHO in the culture medium, while anti-miR-27a significantly accelerated it (Fig. 2C and D).

Similar results were obtained with both HCV-replicating cells

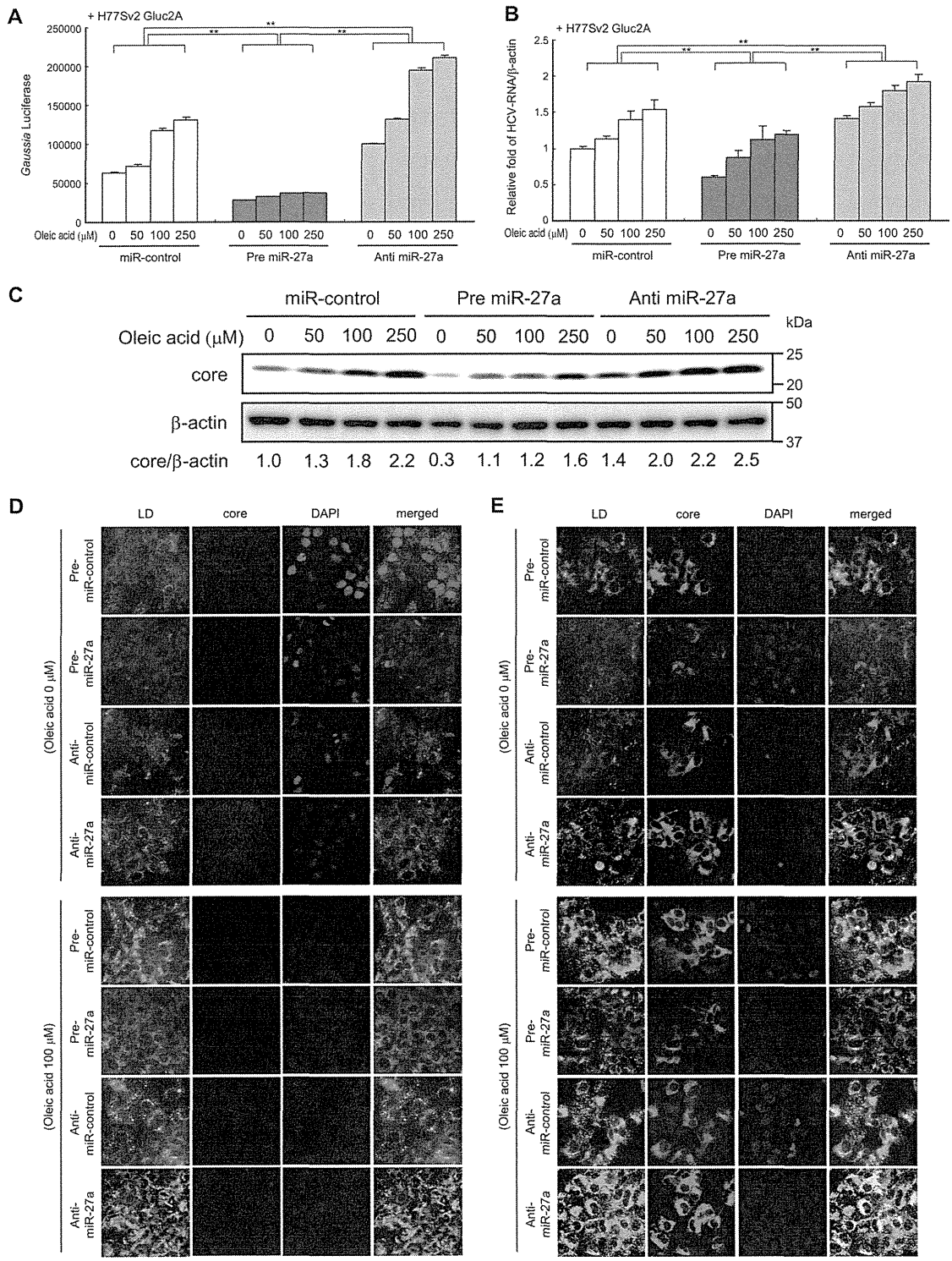

FIG 3 Changes in HCV replication in Huh-7.5 cells caused by pre- and anti-miR-27. Huh-7.5 cells were transfected with H77Sv2 Gluc2A RNA or H77Sv2 Gluc2A (AAG) RNA and pre- or anti-miR-27a. At 24 h posttransfection, increasing amounts of oleic acid (0 to 250 μM) were added to the culture medium. At 72 h after oleic acid treatment, the cells were harvested. (A) Gluc activity in the medium reflecting HCV replication in cells ($n = 6$). (B) Effects of pre- or anti-miR-27 on HCV RNA levels (RTD-PCR, $n = 6$). Experiments were performed in duplicate and repeated three times. Values are means ± standard errors. *, $P < 0.01$; **, $P < 0.005$. (C) Western blotting of HCV core protein in the same experiments. (D and E) Confocal microscopy images of Huh-7.5 cells in the same experiments. D, +H77Sv2 Gluc2A (AAG); E, +H77Sv2 Gluc2A. Cells were fixed, permeabilized, and stained with an anti-HCV core protein antibody. Nuclei were labeled with DAPI. LDs were visualized with BODIPY 493/503 dye. Imaging was performed with a CSU-X1 confocal microscope.

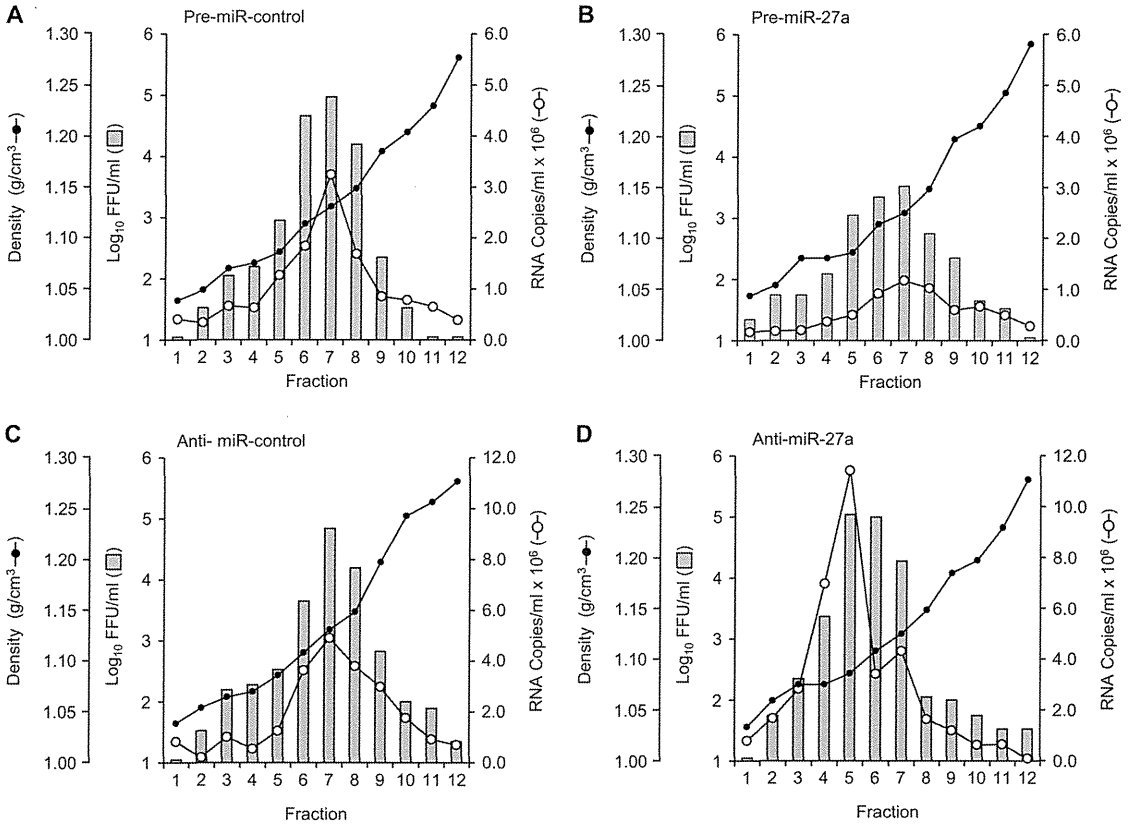

FIG 4 Equilibrium ultracentrifugation of JFH-1 particles in isopycnic iodixanol gradients. Filtered supernatant fluids collected from JFH-1 RNA- and pre- or anti-miRNA-transfected Huh-7.5 cell cultures were concentrated and used to collect fractions (500 μl each). Black circles indicate the gradient densities of the fractions, white circles indicate the HCV RNA titers, and bars indicate HCV infectivity levels. Panels: A, cells overexpressing pre-miR-control; B, cells overexpressing pre-miR-27a; C, cells overexpressing anti-miR-control; D, cells overexpressing anti-miR-27a. Experiments were repeated twice.

(+HCV) (Fig. 2A to D) and non-HCV-replicating cells (+AAG) (Fig. 2E), although the changes in the levels of TG and TCHO in the culture medium were smaller for the non-HCV-replicating cells (+AAG) (Fig. 2E). Correlating with the lipid component findings, replication of the infectious HCV clone H77Sv2 Gluc2A (21), as determined by Gluc activity in the culture medium, and the HCV RNA titer were significantly repressed by pre-miR-27a and increased by anti-miR-27a (Fig. 3A and B). This result was also confirmed by the core protein levels determined by Western blotting (Fig. 3C).

The localization of LDs and core proteins in the cells was visualized by confocal laser microscopy with a lipotropic fluorescent dye and immunostaining of the core protein (Fig. 3E). The LD and core protein levels were substantially repressed by pre-miR-27a and greatly increased by anti-miR-27a antibody. The change in the levels of LDs caused by miR-27a was observed in both HCV-replicating cells (Fig. 3E) and non-HCV-replicating cells (Fig. 3D), although the magnitude of the change was more prominent in HCV-replicating cells.

miR-27a changes the buoyant density and infectivity of HCV particles. The culture medium of Huh-7.5 cells in which JFH-1 was replicating was fractionated by iodixanol gradient centrifugation, and the buoyant density of HCV particles was evaluated (Fig. 4). When the cells were transfected with control miRNA (pre-miR-control and anti-miR-control), the HCV RNA titer (number of copies/ml) and infectivity (number of FFU/ml) peaked at fraction 7 (Fig. 4A and D) and the buoyant density of HCV was estimated at around 1.13 g/cm^3. Transfection with pre-miR-27a did not change the buoyant density of HCV, but it reduced the HCV RNA titer to 0.25-fold of the control and HCV infectivity to 0.024-fold of the control (Fig. 4B). In contrast, transfection with anti-miR-27a reduced the buoyant density of HCV from 1.13 to 1.08 g/cm^3 (Fig. 4B) and increased the HCV RNA titer to 2.1-fold of the control and infectivity to 2.5-fold of the control (Fig. 4C and D). Thus, miR-27a changed the buoyant density and infectivity of HCV.

miR-27a regulates lipid metabolism-related gene expression. The regulation of lipid metabolism-related genes by miR-27a was evaluated in Huh-7.5 cells (Fig. 5 and 6). The lipid synthesis transcription factors PPARγ, FASN, SREBP1, SREBP2, and RXRα were slightly, but significantly, induced in cells in which H77Sv2 Gluc2A replicated. The expression of lipid synthesis transcription factors was compared with that from cells carrying replication-incompetent H77Sv2 Gluc2A (AAG) (Fig. 5 and 6). Unexpectedly, lipid overload with oleic acid had no effect or rather decreased the levels of these transcription factors in non-HCV-replicating cells, probably because of negative feedback mechanisms. Conversely, in HCV-replicating cells, lipid overload with oleic acid further increased the levels of these transcription factors at both the

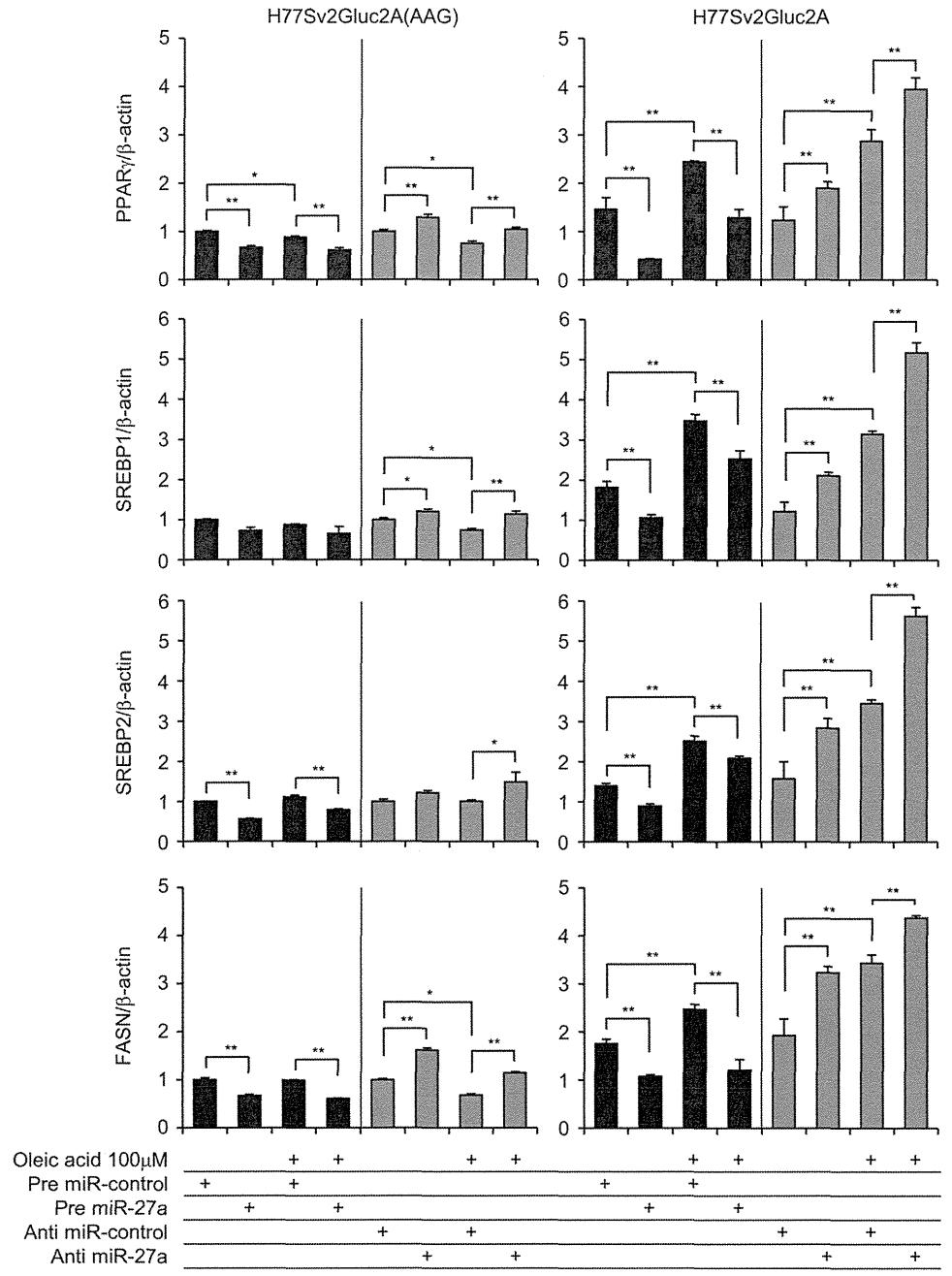

FIG 5 Expression of lipid metabolism-related transcription factors. Huh-7.5 cells were transfected with H77Sv2 Gluc2A RNA or H77Sv2 Gluc2A (AAG) RNA and pre- or anti-miR-27a. At 24 h posttransfection, oleic acid (100 μM) was added to the culture medium, and at 72 h after oleic acid treatment, *PPARγ*, *SREBP1*, *SREBP2*, and *FASN* expression levels were quantified by RTD-PCR ($n = 6$). Experiments were performed in duplicate and repeated three times. Values are means ± standard errors. *, $P < 0.01$; **, $P < 0.005$.

mRNA and protein levels (Fig. 5 and 6A and B). Pre-miR-27a significantly repressed the levels of these transcription factors and, conversely, anti-miR-27a significantly increased their mRNA and protein levels (Fig. 5 and 6A and B). This regulation by miR-27a was observed in both HCV-replicating and non-HCV-replicating cells, although the magnitude of the change was more prominent in HCV-replicating cells (Fig. 5).

As LDs associate with the ER-derived membrane at the site of HCV replication (10) and ER stress was recently shown to promote hepatic lipogenesis and LD formation (31), we next evaluated ER stress markers. Under HCV replication and lipid overload with oleic acid, anti-miR-27a increased the expression of the ER stress markers p-PERK, p-eIF2α, and BiP in Huh-7.5 cells. Conversely, pre-miR-27a significantly decreased the expression of these markers (Fig. 6C). Cell viability decreased after anti-miR-27a transfection and increased following pre-miR-27a treatment (Fig. 6D). Thus, miR-27a repressed the ER stress that was induced by HCV replication and lipid overload.

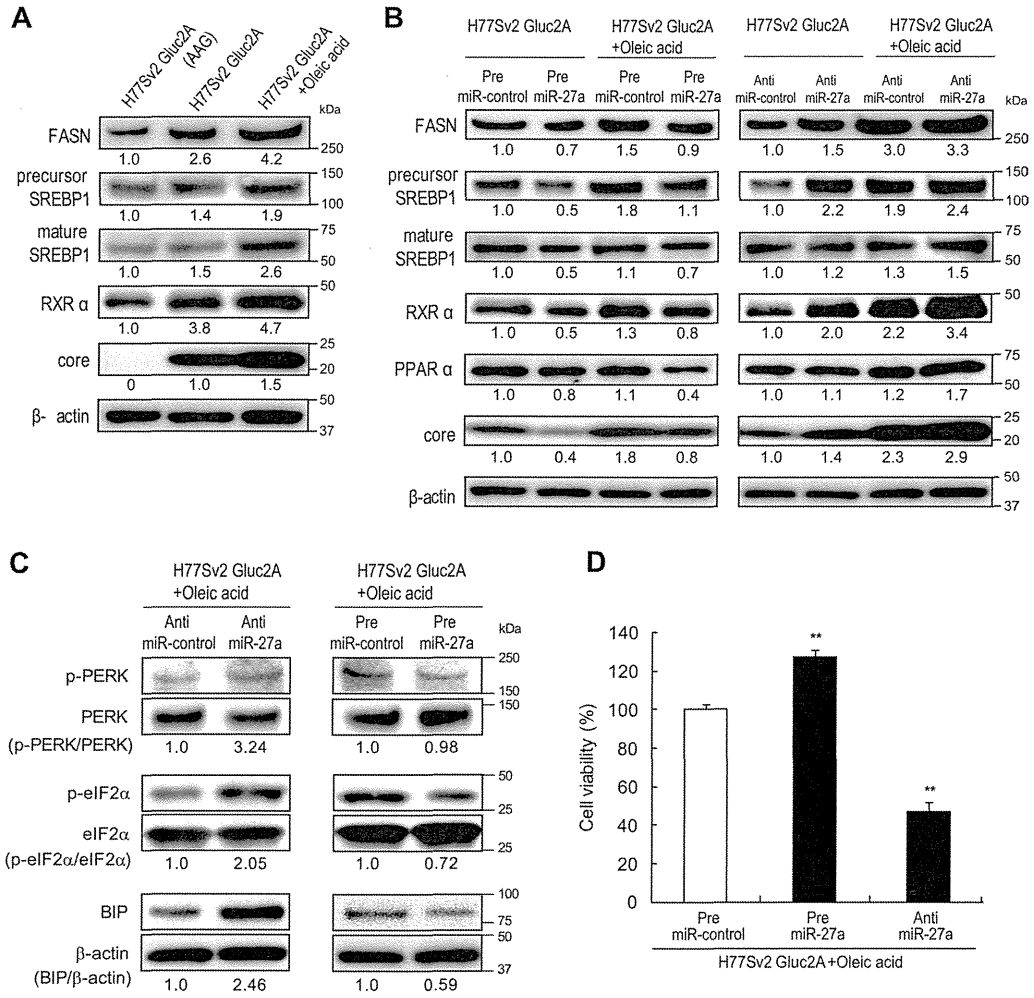

FIG 6 Expression of lipid metabolism-related transcription factors and ER stress-related factors. Huh-7.5 cells were transfected with H77Sv2 Gluc2A RNA or H77Sv2 Gluc2A (AAG) RNA and pre- or anti-miR-27a. At 24 h posttransfection, oleic acid (100 μM) was added to the culture medium. At 72 h after oleic acid treatment, the cells were harvested. (A) Western blotting of lipid metabolism-related transcription factors changed by HCV infection and oleic acid. Experiments were repeated three times. (B) Western blotting of lipid metabolism-related transcription factors changed by pre- or anti-miR-27a. Experiments were repeated three times. (C) Western blotting of ER stress-related transcription factors changed by pre- or anti-miR-27a. Experiments were repeated three times. (D) Cell viability in the same experiments was determined by MTS assay ($n = 9$). Experiments were performed in triplicate and repeated three times. Values are means ± standard errors. *, $P < 0.01$; **, $P < 0.005$.

miR-27a targets RXRα and the ATP-binding cassette transporter ABCA1. We next analyzed the expression of miR-27a target genes. A previous report showed that miR-27a targets RXRα in rat hepatic stellate cells (32), and we confirmed that miR-27a targets the 3′ UTR of human RXRα in Huh-7.5 cells (data not shown). Although the primary sequence of the human RXRα 3′ UTR shares approximately 60% homology with the corresponding rat sequence, the putative miR-27a binding site (ACUGUGAA) is conserved among several different species. Therefore, we constructed an expression vector containing a luciferase (Luc) reporter gene fused to the human RXRα 3′ UTR (pmirGLO-RXRα 3′ UTR) and reevaluated Luc activity (data not shown). Pre-miR-27a repressed Luc activity, while anti-miR-27a significantly increased Luc activity. The introduction of three nucleotide mutations into the conserved miR-27a binding site was shown to abolish these changes in Luc activity. These results confirmed previous findings that miR-27a targets RXRα (32). RXRα interacts with liver X receptor (LXR) and regulates many lipid synthetic genes such as *SREBP1* and *FASN*. We found that the expression of *SREBP1*, *FASN*, and *SREBP2* was regulated by miR-27a (Fig. 6B) and confirmed that *PPARγ* was also regulated by miR-27a, as reported previously (Fig. 5) (33). In addition, *PPARα* was shown to be regulated by miR-27a (Fig. 6B).

We next evaluated the expression of lipid transporter genes. The ATP-binding cassette transporter ABCA1 is mutated in Tangier's disease (34) and plays an important role in the efflux of TCHO for high-density lipoprotein (HDL) synthesis (35). A recent report demonstrated a functional role for ABCA1 in hepatocyte TG secretion to the plasma and in the reduction of cellular TG levels (29). Here we found that pre-miR-27a significantly repressed ABCA1 and, conversely, that anti-miR-27a increased the mRNA and protein levels of ABCA1 (Fig. 7A and B). We identified two miR-27a binding sites (sites 1 and 2) in the 3′ UTR of ABCA1 (Fig. 7C) that were conserved between species (Fig. 7C). An expression vector containing the *luc* reporter gene fused to the human ABCA1 3′ UTR (wild type [WT]) was constructed, and a

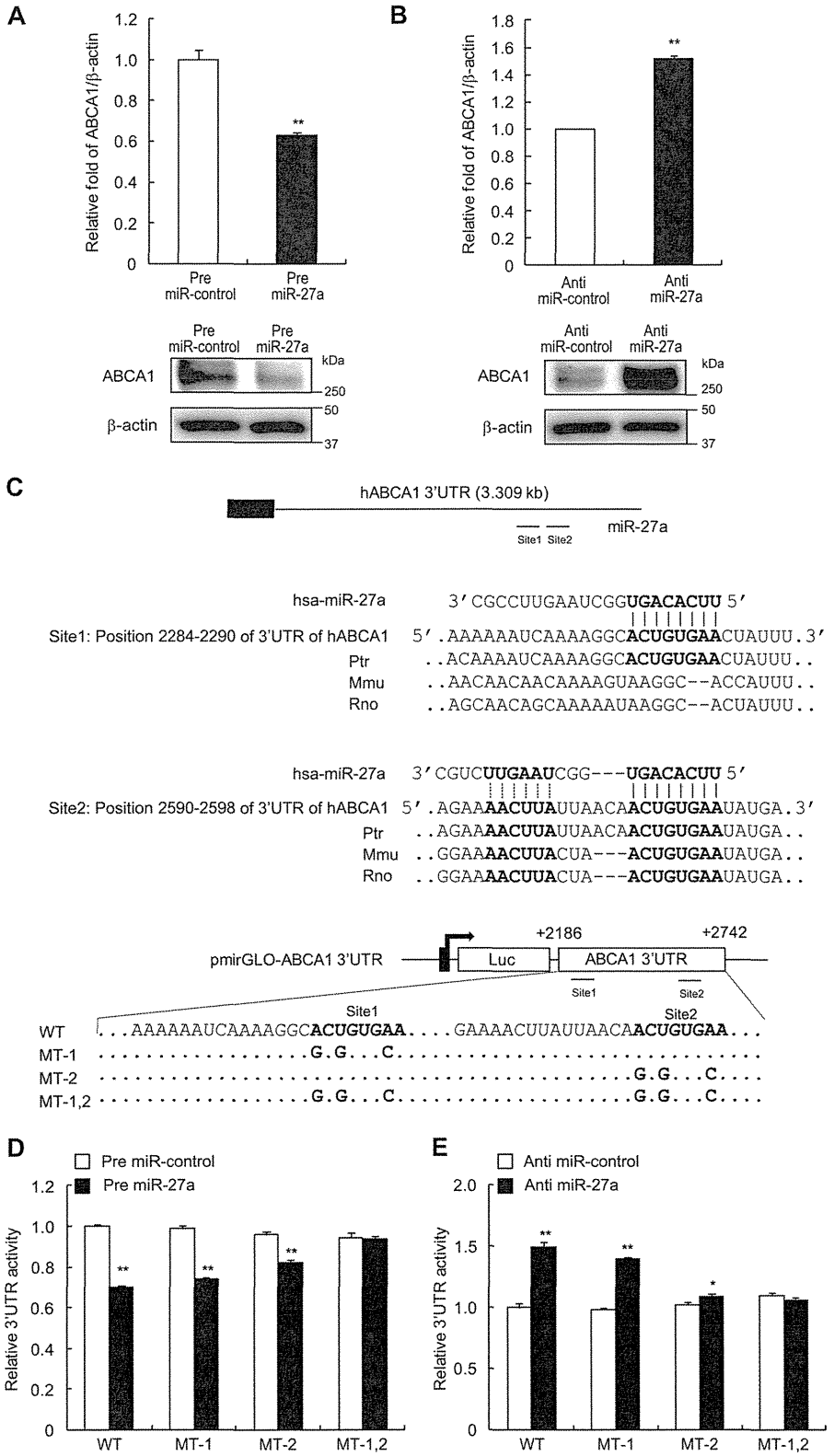

FIG 7 miR-27a targets ABCA1. (A) Regulation of ABCA1 by pre-miR-27a. RTD-PCR and Western blotting of ABCA1 in Huh-7.5 cells at 72 h posttransfection with pre-miR-control and pre-miR-27a ($n = 6$). **, $P < 0.005$. (B) Regulation of ABCA1 by anti-miR-27a. RTD-PCR and Western blotting of ABCA1 in Huh-7.5 cells at 72 h posttransfection with pre-miR-control and anti-miR-27a ($n = 6$). **, $P < 0.005$. (C) Sequence alignment of the ABCA1 3′ UTR and the construction of the luciferase (Luc) expression vector fused to the ABCA1 3′ UTR. Ptr, *Pan troglodytes*; Mmu, *Mus musculus*; Rno, *Rattus norvegicus*; WT, Luc reporter vector with the WT ABCA1 3′ UTR (2186 to 2742); MT-1, Luc reporter vector with the site 1 mutation of the WT; MT-2, Luc reporter vector with the site 2 mutation of the WT; MT-1,2, Luc reporter vector with mutations at sites 1 and 2 of the WT. (D, E) Suppression (D) or induction (E) of Luc activity with the various mutations of the ABCA1 3′ UTR by pre-miR-27a. Huh-7.5 cells were transfected with pre- or anti-miR-control or pre- or anti-miR-27a, and WT, MT-1, MT-2, and MT-1,2. Luc activities were measured at 24 h posttransfection ($n = 6$). All experiments were performed in duplicate and repeated three times. Values are means ± standard errors. *, $P < 0.01$; **, $P < 0.005$.

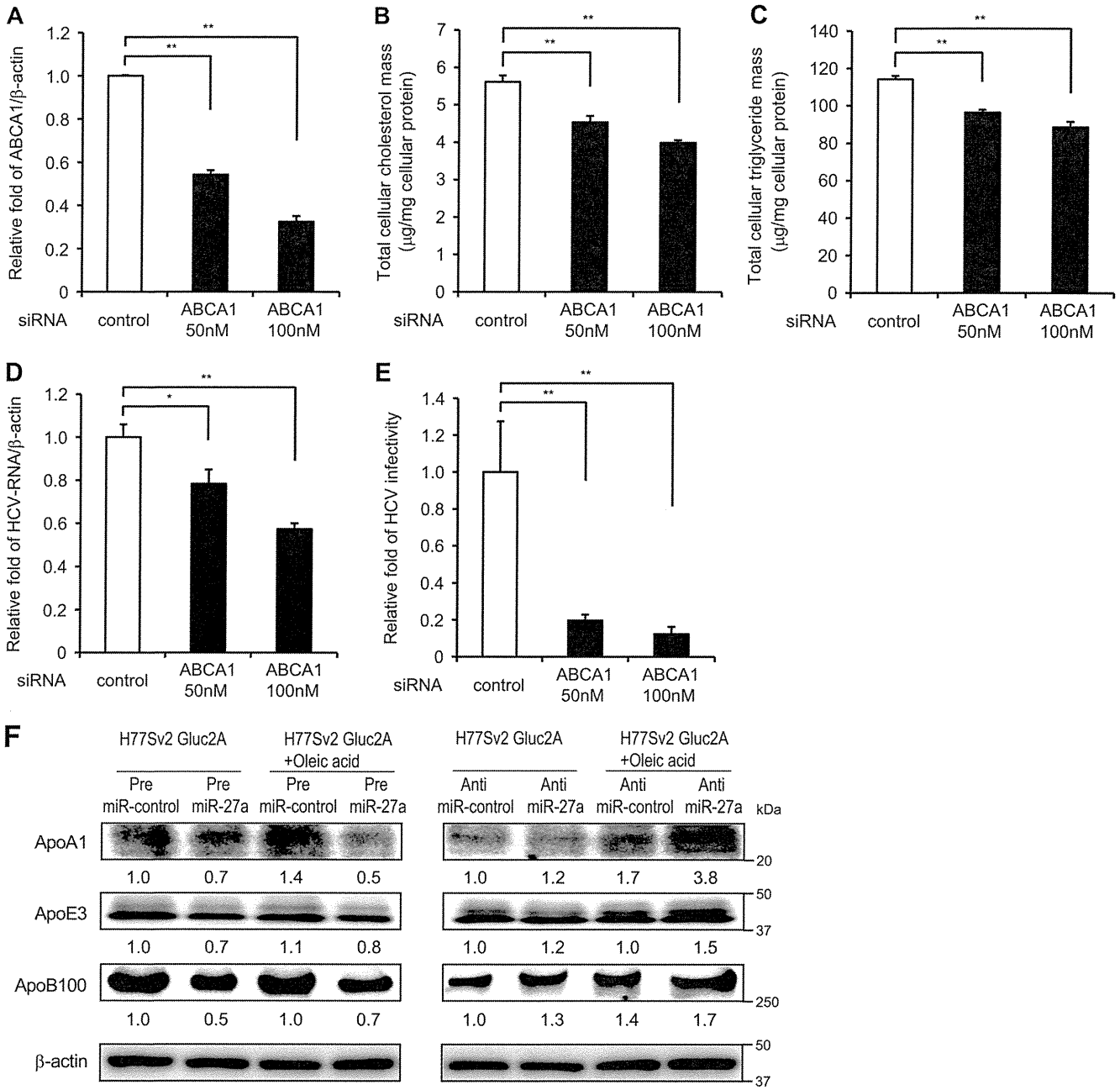

FIG 8 Suppression of ABCA1 inhibits HCV replication and infection. Huh-7.5 cells were transfected with H77Sv2 Gluc2A RNA and siRNA to ABCA1 or control siRNA. ABCA1 expression was quantified at 72 h posttransfection by RTD-PCR ($n = 6$). (A) Knockdown efficiency of ABCA1 in Huh-7.5 cells by siRNA. (B) TG concentration in cells ($n = 6$). (C) TCHO concentrations in cells ($n = 6$). (D) HCV RNA assay by RTD-PCR ($n = 6$). (E) HCV infectivity. Huh-7.5 cells were infected with HCVcc derived from ABCA1 knockdown Huh-7.5 cells. HCV RNA was quantified at 72 h postinfection by RTD-PCR ($n = 6$). Experiments were performed in duplicate and repeated three times. Values are means ± standard errors. *, $P < 0.01$; **, $P < 0.005$. (F) Regulation of ApoA1, ApoE2, and ApoB100 by miR-27a. Experiments were performed under the same conditions as Fig. 6B and C and repeated three times.

series of mutations were introduced into the putative miR-27a binding sites (MT-1, MT-2, and MT-1,2). The Luc activity of the WT was significantly repressed by pre-miR-27a and increased by anti-miR-27a. However, there was a smaller change in Luc activity caused by pre- and anti-miR-27a in the single mutants (MT-1 and MT-2) and no change in Luc activity in the double mutant (MT-1,2) (Fig. 7D and E). These results show that miR-27a targets ABCA1 to decrease the lipid content of cells.

The functional relevance of ABCA1 in lipid metabolism and HCV replication in Huh-7.5 cells was examined by inhibiting ABCA1 with an siRNA (Fig. 8). siRNA to ABCA1 repressed the expression of ABCA1 in a dose-dependent manner (Fig. 8A). Under this condition, the cellular TG and TCHO levels decreased significantly (Fig. 8B and C) and HCV RNA levels also decreased to 57% of the control. More strikingly, HCV infectivity decreased to 12% of the control (Fig. 8D and E).